Universiteit Leiden

Master Computer Science

Decoding 3D Upper Limb Motion Using EEG and Motion Capture: A Deep Learning Approach

Name: Mohamad Hoteit
Student ID: s3564037

Date: April 2025

Specialisation: Artificial Intelligence

Advisor: Richard van Dijk
1st supervisor: Matthijs van Leeuwen
2nd supervisor: Tessa Verhoef

Master's Thesis in Computer Science

Leiden Institute of Advanced Computer Science
Leiden University
Einsteinweg 55
2333 CA Leiden
The Netherlands

Chapter 1

Abstract

BCIs hold promise for translating neural activity into control of external devices, yet most motor-decoding studies have been limited to discrete classification or unreliable continuous trajectories. This thesis explores continuous decoding of executed and imagined upper-limb movements from EEG using both empirical and theoretical approaches. In Part A, a multimodal experimental pipeline was developed to synchronously record 32-channel EEG and MoCap data during both actual and imagined reaching tasks. Despite rigorous preprocessing and synchronization validation, residual EEG artifacts and integration drift in motion data rendered the self-collected dataset unsuitable for training reliable deep learning models. As such, the focus shifted to Part B, where we switched to using the WAY-EEG-GAL public motor-EEG dataset and a new "manifold learning" method called MARBLE. We conducted two reproducibility studies and one original experiment: (1) we verified MARBLE's ability to learn smooth latent embeddings on synthetic vector fields, (2) we replicated its performance on macaque intracranial data by clustering reach directions and reconstructing kinematics, and (3) we performed a novel application of the framework to EEG data, identifying necessary preprocessing steps and running preliminary models to assess compatibility. The findings of this thesis establish both a practical foundation for future data collection and a theoretical basis for structured, geometry-aware decoding strategies that align with the brain's organization of motor intent.

Chapter 2

Acknowledgments

I would like to express my deepest gratitude to my daily advisor, Richard van Dijk, for his invaluable support, patience, and expert guidance throughout my research and writing process. I also wish to thank my supervisors, Matthijs van Leeuwen and Tessa Verhoef, for their insightful comments and suggestions that enriched this work.

My thanks also go to my research lab colleagues, especially Evert Dekker, Jarik den Hartog, and Michel Sjollema, for their assistance with data collection and for many motivating discussions that helped shape this study.

Finally, I am immensely grateful to my family and friends, who encouraged me throughout this journey, for their unwavering support and understanding.

Acronyms

BCI Brain-Computer Interface. 1, 7, 11, 21, 22, 26, 30, 73

BNC Bayonet Neill–Concelman. 7, 35–39

CMS Common Mode Sense. 33

DMP Data Management Plan. 25

DMP Dynamic Movement Primitive. 15–17, 44

DPIA Data Protection Impact Assessment. 25

DRL Driven Right Leg. 33

EEG electroencephalography. 1, 12, 14–16, 18, 21, 24–26, 28, 30, 32–37, 40–46, 48–51, 54–60, 62–73

EHI Edinburgh Handedness Inventory. 24

EMF Electromagnetic Interference. 63, 64

EMG Electromyography. 15

EOG Electrooculogram. 33, 42, 60

GDPR General Data Protection Regulation. 25

IBI Inter-Block Interval. 32, 43

ICA Independent Component Analysis. 59–61

IMU Inertial Measurement Unit. 33, 42

KF Kalman Filter. 14

KRR Kernel Ridge Regression. 14

KVIQ Kinesthetic and Visual Imagery Questionnaire. 25

LFADS Latent Factor Analysis via Dynamical Systems. 18

LPT Line Printer Terminal. 38

LSL Lab Streaming Layer. 37

ME Motor Execution. 7, 21, 22

MI Motor Imagery. 7, 21, 22

MLR Multivariate Linear Regression. 14

MoCap Motion Capture. 1, 12, 24–26, 28, 32–37, 40–42, 48, 49, 51, 54, 57, 58, 64, 72, 73

MTRT Motion Trajectory Reconstruction Trasnformer. 15

P Preparation. 32

PCA Principal Component Analysis. 68, 69, 71

PTT Pursuit Tracking Task. 22

R Rest. 32

T Trial Execution. 32

TTL Transistor-Transistor Logic. 7, 36–38, 56

V Visual Message. 32

VR Virtual Reality. 14

ZUPT Zero Velocity Update. 63

Contents

List of Figures

List of Tables

Chapter 3

Introduction

3.1 Motivation and Research Objective

Brain-Computer Interfaces (BCIs) provide a way to translate neural activity from the brain into commands for external devices. This offers exciting oportunities for assistive technologies, neuro-rehabilitation, and immersive virtual experiences [Sosnik and Zheng, 2021]. Accurately interpreting motor intentions from brain signals into natural movement remains one of the main challenges in BCI research.

Traditionally, BCI studies employ classification approaches in solving the motor decoding challenge. This approach categorizes predefined movements or imagined actions into discrete classes [Lotte et al., 2018]. While this approach can be effective, it still fails in providing the full dynamic nature of real-world movements. A different paradigm, namely trajectory reconstruction, has aimed to address this limitation through the continuous estimation of movement parameters such as limb velocities from neural activity [Sosnik and Zheng, 2021, Robinson et al., 2015, Korik et al., 2019, Jeong et al., 2020].

Previous studies demonstrated the ability of decoding continuous trajectories using linear models (see Section 4.1.1). Unfortunately, performance was limited, especially in the case of imagined movements. More recent work has shown that deep learning models, especially those combining spatial and temporal components, can improve decoding accuracy for executed movements [Pancholi et al., 2022]. However, their application to imagined movements has not been explored. This thesis aims to address this discrepancy by investigating whether these models can also improve the accuracy of decoding imagined upper limb movements in a continuous manner. Additionally, we are interested in checking whether decoding performance can be improved by targeting biomechanically meaningful variables. In other terms, we would like to investigate how decoding performance varies between choosing velocities, positions or joint angles as the decoding target [Wang et al., 2023c].

3.2 Research Question

This work was guided by the following central research question:

> *Can deep learning models accurately decode both continuous executed and imagined upper limb movements from EEG signals, and what representations or modeling strategies are best suited for this task?*

To address this, the thesis is structured into two complementary parts:

- **Part A:** A hands-on approach that aims to build a pipeline for simultaneous recording and preprocessing of electroencephalography (EEG) and Motion Capture (MoCap) data to train models that decode physical movement.
- **Part B:** An exploration into how the brain might internally represent movement. The goal is to determine the best modeling approach in order to address the limitations in the literature.

3.3 Part A: Experimental Approach – End-to-End Deep Learning for Motion Decoding

Part A initially aimed to implement an end-to-end deep learning pipeline that allows for decoding upper limb trajectories from synchronized EEG and MoCap recordings. The experiment involved both executed and imagined movements, with a focus on using deep learning models, such as CNN-LSTMs or transformers, that can capture spatiotemporal dynamics in neural activity. The latter would be used to reconstruct movement trajectories directly from EEG signals. The aim was to extend previous work by applying these models to imagined movements.

However, despite careful planning, our approach was limited by real-world constraints. This included hardware limitations, which had a negative impact on data quality and work scheduling. As a result, the collected dataset was deemed unsuitable for our purposes. This forced us to reconsider our methodology, pushing us towards a deeper investigation onto how motor intention is represented in the brain.

3.4 Part B: Theoretical Approach – Modeling Internal Motor Representations

Building on insights from the initial phase, Part B focuses on identifying the most suitable modeling approach to achieve our goal. This required an extensive investigation onto movement representation in the brain. Our initial goal of decoding physical positions was replaced by an understanding that movement representation is better captured by interpreting it as patterns of activity that follow an organized and structured path in a simplified, low-dimensional latent space. This shift was mainly driven by our goal of improving reconstruction of imagined trajectories, which would have been limited had we followed our initial intuitions from Part A.

This part explores alternative modeling strategies using latent space representations, contrastive learning, and manifold geometry. It makes use of theoretical models such as MARBLE, originally developed for invasive neural data, and attempts to adapt their insights for use with EEG. A public dataset was used as temporary stand-in for our own recordings to explore the feasibility of inferring imagined trajectories from neural signals, and to investigate the model's ability to generalize to unseen trials and new motor intentions.

Although practical implementation of these models was constrained by time and scope, this theoretical trajectory offers a strong foundation for future empirical work.

3.5 Thesis Outline

This thesis reflects two bodies of work: one about building and testing a real system, and another about developing the theory that completes it. Each main chapter is split into two parts to reflect this structure.

- **Chapter 4 – Related Work:** Provides a literature review onto concepts relevant to both standard motion decoding and models of motor representation.
- **Chapter 5 – Background:** Provides knowledge to familiarize the reader with some preliminary information related to motor decoding.
- **Chapter 6 – Methodology:** Details the experimental approach and theoretical modeling approach.
- **Chapter 7 – Experiments:** Provides a high-level description of experiments conducted during pipeline construction, and during empirical exploration of our new modeling approach using our recordings (Part A) and public datasets (Part B).
- **Chapter 8 – Results:** Presents the results of the experiments introduced in the previous chapter.
- **Chapter 9 – Discussion:** Merges insights from Parts A and B, reflecting on their interplay.
- **Chapter 10 – Conclusion:** Summarizes contributions and proposes future directions.

Chapter 4

Related Work

This chapter provides the foundation for both phases of the thesis. It is structured in two parts, reflecting the dual progression of the project. Part A looks at the practical work and ideas that shaped the experiment. It reviews prior work on EEG-based trajectory decoding, including linear models and early deep learning strategies. It also examines the biomechanical and neural control principles that guided the selection of decoding targets and inspired the experimental design. While Part B explores the theoretical shift that followed the practical challenges encountered during implementation. It also introduces recent theoretical advancements in movement representation, such as neural manifolds, reference frame transformations, and compositional motor structures. These insights offered a more structured way to conceptualize motor intention and laid the groundwork for future decoding models.

4.1 Part A: Theoretical Basis for Experimental Approach

4.1.1 Initial Approaches to EEG-Based Movement Decoding

The original hypothesis aimed to decode EEG signals into upper-limb movement trajectories using deep learning models. This work is motivated by studies employing linear models such as Multivariate Linear Regression (MLR), Kernel Ridge Regression (KRR), and Kalman Filter (KF) as per [Sosnik and Zheng, 2021, Robinson et al., 2021, Korik et al., 2019, Kobler et al., 2020]. These studies emphasized the correlation between velocity and low-frequency EEG. The decision to explore deep learning models was primarily inspired by the promising results reported by Pancholi et al. [2022]. The latter showed superior performance over in decoding 3D hand trajectories using a hybrid CNN-LSTM model.

4.1.2 From Classification to Continuous Trajectory Reconstruction

A important conceptual distinction emerged during the literature review between classification-based decoding [Lotte et al., 2018], common in motor imagery research, and continuous trajectory reconstruction, which is more suitable for practical applications such as Virtual Reality (VR) embodiment or motor rehabilitation. Continuous decoding methods [Sosnik and Zheng, 2021, Pancholi et al., 2022], offering natural and fluid movement control, were thus prioritized for their practical aspect.

4.1.3 Biomechanical Constraints & Decoding Modality

The Motion Trajectory Reconstruction Trasnformer (MTRT) by Wang et al. [2023c], highlighted the value of biomechanical constraints on decoding performance. The loss function employed by their model included constraints on the decoded position that were in line with the acceptable range of motion of the average human. As such, we consider the potential performance improvement from applying such constaints on decoding targets such as joint angles, positions, and velocities.

4.1.4 Movement Primitives as Biomechanical Intermediaries

Investigating neuromusculoskeletal models, particularly the Electromyography (EMG)-driven musculoskeletal model introduced by Durandau et al. [2018], revealed how internal biomechanical variables contribute to movement. Their framework broke down the decoding process several steps, including muscle activation, force generation, and finally joint movement. This hinted at how brain signals might translate into physical motion. Velocity becomes an informative decoding target that naturally integrates components like muscle activation and joint torques. To be clear, although velocity does not explicitly represent muscle activations or joint torques, it emerges from their combined effect. As such, velocity can be seen as a high-level feature that implicitly carries information about the underlying neuromuscular control.

In contrast, Vargas et al. [2023] used artificial neural networks trained on simulated muscle spindle input (feedback signal from the muscles to the nervous system) to show that activity in the somatosensory cortex more closely matched variables, such as joint positions and velocities, instead of detailed muscle-level signals. This supports a hierarchy in motor representation, where lower levels (e.g. EMG) reflect fine-grained motor control, while higher levels (e.g. neo-cortex) abstract movement into goal-oriented kinematics. Even though Vargas et al. [2023] studied the somatosensory cortex, we can assume that the motor cortex uses similar ways of representing movement. This assumption is based on the observation that these brain areas are both in constant feedback loops aiming to predict and adjust actions as they happen [Evarts, 1973, Friston, 2010]

These insights led us to consider frameworks capable of representing movement compositionally and hierarchically. Dynamic Movement Primitives (DMPs), for instance, model trajectories using abstract parameters like phase, amplitude, and goal. Hotson et al. [2016] demonstrated that decoding performance improves when such simplified representations are used, suggesting that the brain may construct complex actions by combining simpler movement primitives. This resonated with our early intuition that generalization to unseen movements might rely on an efficient subspace of motor actions, potentially formed from basis vectors or eigencomponents. The DMP framework offered a mathematical formalism that aligned with this view, serving as a bridge between biologically grounded theories and practical modeling tools for exploring modularity and generalization in motor decoding.

Importantly, this compositional structure becomes even more valuable when decoding imagined movements. In the absence of overt muscle activity or sensory feedback, decoding must rely on internal representations that are abstract, stable, and generalizable. DMPs and similar frameworks, by simplifying motion into a small set of dynamic parameters, offer a way to bridge the gap between noisy EEG signals and high-level motor intentions. They also enable the possibility of mapping imagined actions into meaningful trajectories by leveraging shared latent structure across movement types (executed vs imagined). This insight played a key role in shaping both our theoretical and methodological shift toward models that explicitly take advantage of compositionality and latent space structure.

4.1.5 Temporal Synergies and Sequence Models

In recent work, temporal synergies within EEG signals were identified Yoshimura et al. [2017]. These correspond to recurring activation patterns in motor regions. The sequence of activations seems to carry meaning in interpreting motor intentions. This provides additional support for the concept of compositionality. These findings suggest that decoding endeavors could improve by taking advantage of these structured temporal dynamics. Additionally, the phase-driven mechanism in DMPs, which behaves like an internal clock that orchestrates state-transitions, seems to matched the brain's own time-dependant activity patterns. This encourages the use of models that account for long-range temporal dependencies.

In addition to these theoratical insights, empirical efforts were made in recent work to model these temporal dynamics using deep recurrent architectures like ChronoNet [Roy et al., 2022]. Notably, Wang et al. [2023c] used a transformer model, achieving improved decoding performance compared to previous approaches Pancholi et al. [2022], although on a different dataset. With these observations supporting the literature about temporal synergies and DMPs, we were encouraged to explore transformer architectures' ability to capture long-range temporal dependencies in EEG signals. These insights also emphasized the importance of tailoring the choice of deep learning architecture such that it is driven by domain-knowledge, rather than simply increasing the computational potential of the model.

Taken together, these insights point toward a key realization: decoding motor intentions from EEG cannot rely solely on raw coordinate prediction or linear regression. The brain represents movement using structured, low-dimensional, and compositional patterns that abstract away muscle-level details in favor of goal-directed kinematics. These representations are not only hierarchical and temporally organized but also robust to noise and capable of generalizing across tasks. In this context, rather than treating EEG as unstructured input and attempting to force a structure during decoding, it is more advantageous to employ models that take advantage of latent spaces, specifically neural manifolds (more on that in Section 4.2.3). These offer the ability to capture the underlying task-relevant parameters using a structures representation that is more in line with brain-like representations. This synthesis motivated the shift in Part B: from learning direct mappings to designing decoding models that explicitly recover and align with the internal geometry of motor intention as reflected in EEG.

4.2 Part B: Theoretical Framework for Structured Decoding and Neural Geometry

4.2.1 Movement Primitives as Goal-Directed Dynamical Systems

As discussed in Part A, the DMP framework offers a method for modeling movement as a set of simplified dynamic parameters. These models describe trajectories as goal-directed dynamical systems shaped by a phase variable and internal control parameters [Saveriano et al., 2023, Hotson et al., 2016, Bahl et al., 2020]. The success of this approach at EEG decoding hints at the fact that the brain might employ similar abstractions in motion representation.

4.2.2 Reference Frames in Motor Representation

Yoshimura et al. [2017]'s source localization not only reflected temporal dynamics as discussed in Section 4.1.5, but also highlighted that different brain regions are involved, depending on whether movement is framed intrinsically (body-relative) or extrinsically (world-relative). This aligns with more recent findings which showed that the brain often encodes movement goals in world-centered terms, even if the actual movement is carried out using a body-centered perspective Herweg and Kahana [2018], Ottenhoff et al. [2025]. This dynamic shifting between reference frames reinforces that idea that basic regression into Cartesian coordinates, as has been done in most prior work, can only capture a very limited representation of brain dynamics that correlate with motion. This motivates the use of decoding models capable of internally representing different spatial encodings.

4.2.3 Neural Manifolds and Population Geometry

Before encountering formal manifold literature, our investigations had converged on the idea that motor intent is encoded in structured, compositional neural activity patterns. Our initial thoughts hovered around concepts like DMPs, basis and, eigenvectors as per Section 4.1.4. This was later formalized by Chung and Abbott [2021], who described patterns of brain activity as 'neural trajectories' moving through high-dimensional spaces, known as 'neural manifolds'.

Neural manifolds adapt dynamically through transformations such as rotations, scaling, and non-linear warping, depending on the cognitive context or motor task Chung and Abbott [2021]. For example, when a person reaches for a cup with their right hand versus their left, the brain might use the same general motor plan but represent it differently depending on the hand used or the target's position in space. In this example, the underlying neural activity still follows a similar structure but is reshaped (rotated, stretched, or curved from a neural manifold perspective) to match the specific context. This allows the brain to reuse existing movement patterns, instead of creating a new representation every time. This mechanism mediated by 'neural manifold' was critical for decoding imagined trajectories. Unlike executed movements, imagined actions lack sensory feedback and overt muscle activation. To design a model capable of generalizing to imagined movements, you then need a mechanism to differentiate between more subtle and internally generated neural patterns. These manifold transformations constitute a solid option for detecting these variations in motor representations within the same latent space.

Moreover, this adaptability to different cognitive contexts aligns well with the dynamic switching between spatial reference frames discussed earlier in Section 4.2.2. Just as the brain can shift between allocentric and egocentric representations, decoding models should also exhibit a similar mechanism. This can be achieved by employing manifold-based decoding approaches as they leverage transformations in their latent space. In this way, we can achieve true generalization, by employing methods that mimic the brain's own strategies for integrating context-specific motor intentions.

4.2.4 Latent Space Approaches to EEG Decoding

Building on the manifold framework, we explored models that explicitly learn structured, low-dimensional manifolds from neural data; notably MARBLE and GREEN. Unlike typical latent space models that reduce dimensionality without enforcing structure, manifold learning approaches aim to uncover the underlying geometry and dynamics of neural activity.

MARBLE, originally developed for intracranial neural recordings (i.e., implanted electrodes rather than non-invasive sensors like EEG), uses contrastive learning to embed neural samples as continuous flow fields over a learned manifold [Gosztolai et al., 2025]. This approach builds on earlier models like Latent Factor Analysis via Dynamical Systems (LFADS), which inferred neural trajectories from high-resolution recordings of neuronal populations [Pandarinath et al., 2018]. GREEN adapted manifold learning for EEG by combining Riemannian projections with adaptive wavelets to handle the noisier scalp signals [Paillard et al., 2024].

These studies validated our earlier hypotheses and provided computational tools to formalize them. Although constraints prevented full implementation, these models offer a solid basis for future work.

Chapter 5

Background Information

In this chapter, we provide the reader with some useful background information in order to gain a solid understanding of some of the basic terminology relevant to this type of research.

5.1 Frequency Bands

Cortical activity is reflected in EEG signals across a frequency range from below 4 Hz to approximately 140 Hz. The commonly recognized frequency bands and their associated cognitive or behavioral states are summarized in Table 5.1.

Table 5.1: Summary of EEG frequency bands and their associated cognitive or behavioral states.

Wave Type	Frequency Range	Associated State / Function
Delta	< 4 Hz	Deep sleep
Theta	4–7 Hz	Light sleep, drowsiness, hypnagogic states
Alpha	8–12 Hz	Relaxed wakefulness, eyes closed
Mu	7.5–12.5 Hz	Motor cortex activity, motor imagery and execution
Low Beta	12.5–16 Hz	Focused attention, alertness
Beta 2	16.5–20 Hz	Active thinking, cognitive load
High Beta	20.5–28 Hz	High alertness, anxiety, stress
Gamma	25–140 Hz	Higher-order cognition, perception, memory, consciousness

5.2 Brain Areas

The brain is organized into distinct regions that correspond to motor and sensory functions. This distribution is illustrated by the Penfield homunculus in Figure 5.1, which shows how different body parts are mapped to specific areas in the motor and somatosensory cortices.

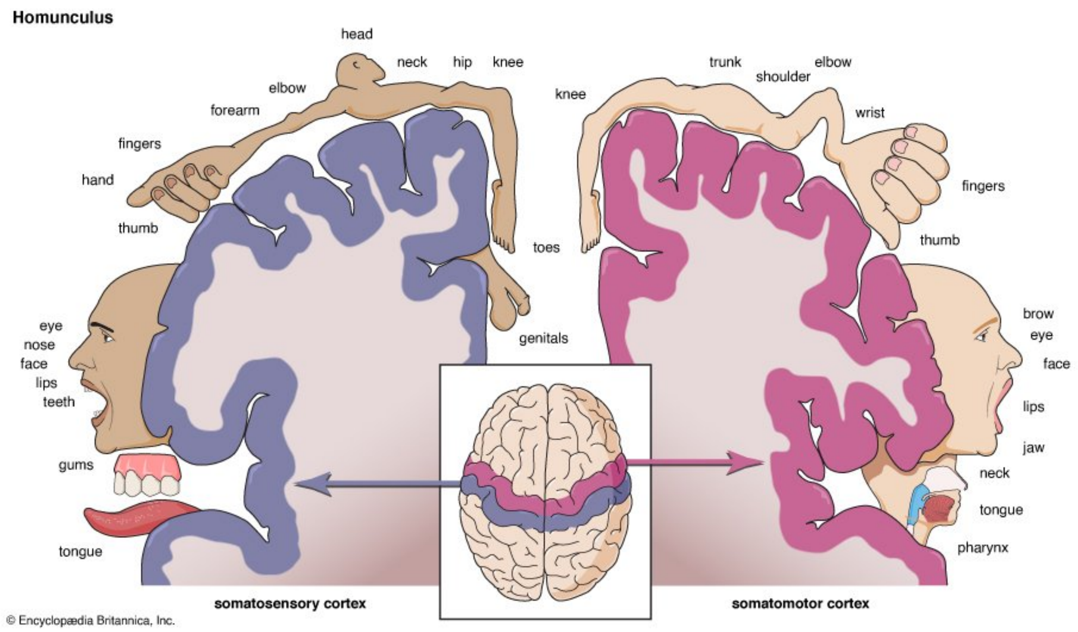

Figure 5.1: Penfield Homunculus. *Credit: Encyclopaedia Britannica*

The somatosensory cortex processes sensory information from the skin, muscles, and joints, while the motor cortex is responsible for planning and executing voluntary movement[Condylis et al., 2020]. Each limb is associated with the contralateral hemisphere—e.g., the left hemisphere controls the right side of the body.

The outer layer of the cerebrum, the cerebral cortex, is divided into Brodmann areas. EEG data is commonly recorded using the 10-10 system, standardized by the American Electroencephalographic Society. Figure 5.2 shows both the 10-10 system aligned with Brodmann areas and the simplified 10-20 layout used in this thesis.

In this thesis, we use a reduced 32-channel montage based on the 10-20 system, as shown in Figure 5.2b, following guidance from recent literature.

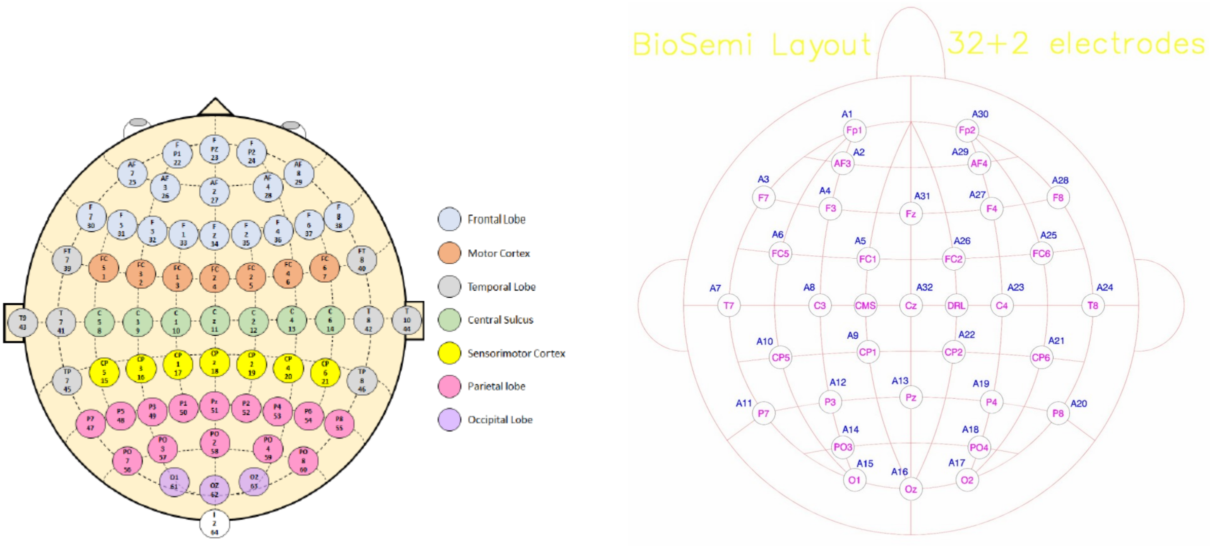

(a) 10-10 system with Brodmann areas. *Credit: [Asanza et al., 2022]*

(b) 32 EEG electrodes (10-20 system). *Credit: [B.V., n.d.]*

Figure 5.2: Comparison of the 10-10 system (left) and the 10-20 system with 32 electrodes (right).

5.3 Experimental Paradigms in Recent Literature

EEG-based BCI studies typically employ motor imagery (MI) or motor execution (ME) paradigms, each with distinct experimental goals.

5.3.1 Motor Imagery (MI) Paradigms

MI refers to the mental simulation of movement without physical execution [Hanakawa et al., 2003]. MI tasks are often categorized as either **kinesthetic**, involving the imagination of the sensation of movement (e.g., muscle tension), or **visual**, involving the mental visualization of movements from a first- or third-person perspective [Neuper et al., 2005].

Common MI tasks include imagining hand, foot, or tongue movements [Edelman et al., 2019, Pfurtscheller et al., 2006]. These tasks align with the somatotopic organization of the motor cortex. While useful for classification, MI-based BCI studies increasingly explore continuous decoding tasks, such as estimating velocity during reaching [Jeong et al., 2020, Kim et al., 2015].

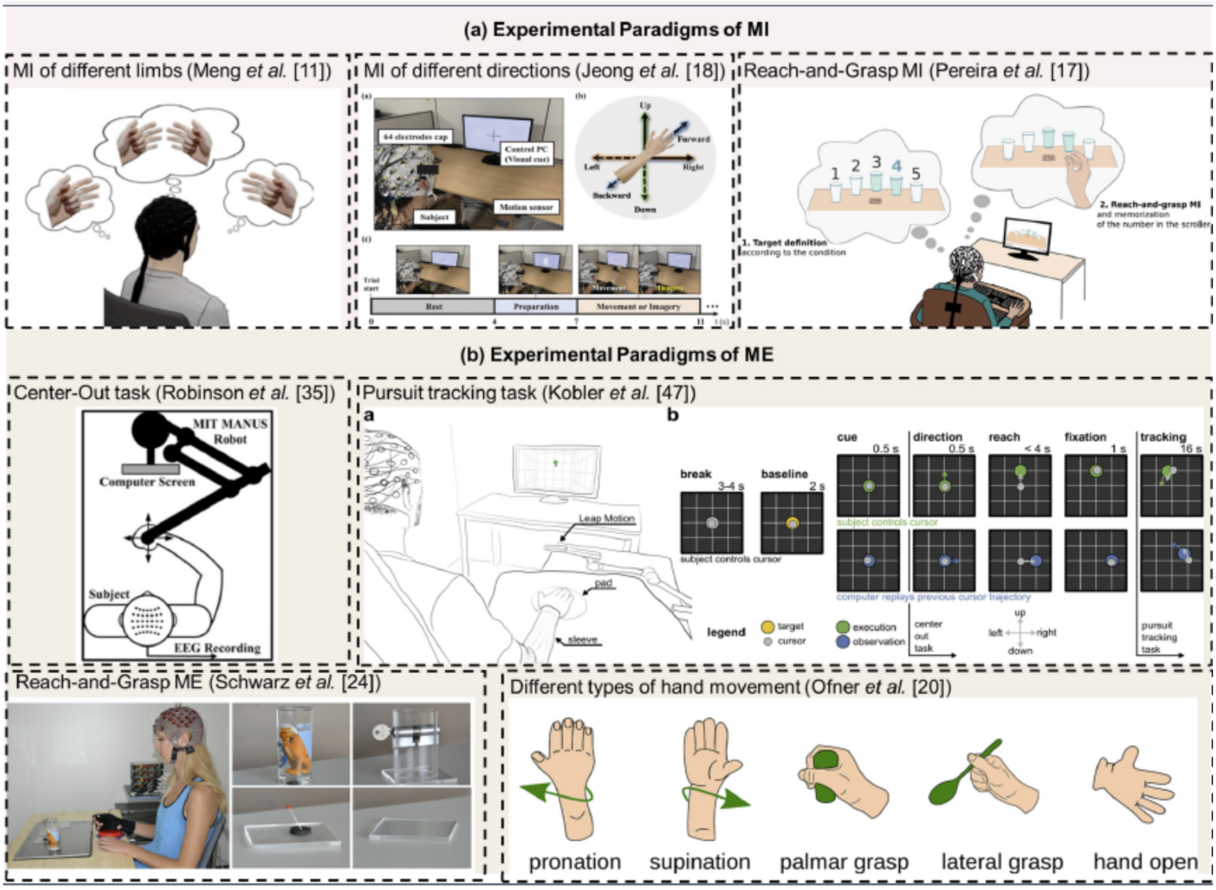

Figure 5.3: Summary of experimental paradigms for upper-limb motor BCI, including (a) MI and (b) ME. *Credit: [Wang et al., 2023b]*

5.3.2 Motor Execution (ME) Paradigms

ME refers to real physical movements and reflects natural motor control [Bai et al., 2007]. ME tasks are often categorized as either **movement type recognition**, which involves identifying movement types such as wrist rotation, elbow flexion, or grasping [Liu et al., 2018], or **movement onset detection**, which involves identifying the intention to move for real-time BCI use [Jochumsen et al., 2015].

Movement decoding experiments often use center-out tasks where participants move from a central position to multiple targets [Robinson et al., 2015, Sosnik and Zheng, 2021, Wang et al., 2022]. Other paradigms include pursuit tracking tasks (Pursuit Tracking Task (PTT)) using cursors to follow moving stimuli. Decoding velocity, direction, and position is possible, though noise and artifacts remain significant challenges.

5.3.3 2D vs. 3D Reconstruction

Reconstruction efforts in EEG-based motion decoding can differ significantly depending on the dimensionality of the targeted movements. In 2D reconstruction, motion is constrained to a planar surface, such as horizontal or vertical movements on a screen. This approach is often simpler to implement and interpret, making it more robust and easier to decode from EEG data due to the reduced complexity of the motion [Robinson et al., 2015, Kim et al., 2015]. In contrast, 3D reconstruction involves estimating motion in three-dimensional space, accounting for additional degrees of freedom such as depth and joint articulation. While 3D reconstruction offers a more realistic and natural representation of upper-limb movements [Sosnik and Zheng, 2021], it poses greater challenges in terms of decoding accuracy and signal reliability, particularly when using non-invasive neuroimaging techniques like EEG [Jeong et al., 2020].

Chapter 6

Methodology

This chapter outlines the methodological framework used in both phases of the thesis. Reflecting the structure of the project, it is divided into two parts. Part A details the design, execution, and technical aspects of the empirical experiment, including hardware-software integration, synchronization strategy, and participant protocol. Part B presents the theoretical modeling plan, including decoding targets, neural representation strategies, and planned model architectures.

6.1 Part A: Experimental Approach – End-to-End Deep Learning for Motion Decoding:

6.1.1 Participant Recruitment and Inclusion Criteria

The study involved healthy adult volunteers recruited primarily from Leiden University, including both students and staff. A total of 10 participants were planned, representing a typical sample size for exploratory EEG studies. Participants were recruited through university mailing lists, posters, and personal networks. All volunteers were required to be 18 years or older and capable of providing informed consent. To maintain consistency in both motor ability and neural activity, only individuals with no history of neurological or musculoskeletal conditions were included.

Beyond these basic health criteria, additional factors were considered to ensure reliable EEG and MoCap recordings:

- **Age Range:** Only participants between the ages of 18 and 35 were included. This range was selected because EEG signal quality and motor control have been shown to decline with age [Dustman et al., 1999, Delgado-Aguilera et al., 2024], and adhering to this range helped to minimize variability across participants and trials.

- **Handedness:** All participants were right-handed, as confirmed using the Edinburgh Handedness Inventory (EHI) as per [Oldfield, 1971]. This was done to ensure consistent brain hemisphere activation during motor tasks, since handedness affects how motor plans are represented in the brain.

- **Session Timing and Meal Instructions:** To control for natural fluctuations in brain activity, all sessions were conducted during a fixed two-hour window in the morning or afternoon. Participants were also instructed to eat a light meal at least one hour before the session, as both time of day and food intake can affect EEG signal patterns [Cajochen et al., 1995].

- **Fit and Compatibility:** Participants underwent visual inspection for factors that could interfere with signal quality or sensor placement, such as very thick hair, unusual skull shape, or body proportions that might distort the MoCap suit fit. These checks were based on guidelines from previous MoCap studies [Liao et al., 2011].

- **Motor Imagery Ability:** Since the experiment included imagined movement tasks, participants were also assessed for their ability to perform different forms of motor imagery (see Section 5.3.1) using the Kinesthetic and Visual Imagery Questionnaire (KVIQ) as per [Malouin et al., 2010]. Only those with scores above a certain threshold were invited to participate.

These criteria helped in noise reduction during EEG recordings sessions and increased the reliability of comparisons between participants. The goal was to recruit a small but carefully selected group of individuals capable of performing both executed and imagined versions of the motor task under controlled conditions.

6.1.2 Ethical Approval and Data Management

This study was conducted in accordance with the ethical standards of Leiden University. Approval was granted by the university's Ethics Committee (see Appendix E), allowing the recruitment of up to ten participants. Additionally, the research went through a formal Data Protection Impact Assessment (DPIA) (DPIA: FWN24-008) to ensure compliance with the General Data Protection Regulation (GDPR). The DPIA outlined the nature of the data collected, including sensitive biometric signals (EEG and MoCap), as well as basic contact information (name, email, student ID). To protect participant privacy, all data were pseudonymized and access was strictly limited to the researcher and supervisor.

Finally, a detailed Data Management Plan (DMP) was also submitted and approved prior to the start of the study. This plan covered how data would be stored, processed, and protected over the course of the project. Key data handling procedures included:

- **Storage:** All data were saved on the university's secure network (J: Drive), with backups and version control handled via descriptive filenames and metadata logs.

- **Encryption:** Sensitive files were encrypted using Veracrypt, and access was restricted to approved devices.

- **Pseudonymization:** Personally identifiable data were stored in a separate location from EEG and MoCap recordings, minimizing the risk of identification.

- **Metadata Documentation:** Data was documented using standardized README files following the ISA-Tab format to ensure reproducibility and clarity for potential collaborators.

- **Retention and Sharing:** In line with university guidelines, the data will be stored for 10 years. While the dataset itself will not be made public due to privacy restrictions, metadata may be shared upon request for purposes of collaboration or verification.

These steps were taken to protect participants' privacy while still being open about the research methods, making sure the study followed both ethical guidelines and proper data handling standards for neuroscience research.

6.1.3 Data Collection Experiment Refinement

This section describes the process of iteratively improving our experimental design, shaped by a combination of practical constraints, literature insights, and iterative pilot testing. Our aim was to develop a setup that could capture both EEG and MoCap data during upper-limb executed and imagined movements, while ensuring a comfortable experience for participants.

EEG System Selection

Choosing the right EEG system was a crucial step. We needed a device that could deliver high-quality neural recordings, work smoothly with MoCap systems, and support precise synchronization. We began with a literature review focused on EEG systems commonly used in BCIs and neurorehabilitation research. A survey by Dai et al. [2023] proved especially useful, as it compared popular systems in terms of signal quality, number of channels, portability, and synchronization support (see Table 6.1). This gave us a solid benchmark for evaluating options.

With this information, we contacted vendors like ANT Neuro and Artinis, two Dutch companies with strong reputations in the field. We scheduled meetings to explore technical specifications, potential university-mediated discounts, and/or short-term lease possibilities. At the same time, we investigated existing EEG setups already available at Leiden University. This involved visiting labs, reviewing inventories, and consulting with technical staff.

Following our vendor meetings, it became clear that both ANT Neuro and Artinis offered excellent systems in terms of channel density, signal quality, and synchronization support. ANT Neuro in particular provided compelling advantages with active electrodes, portable amplifiers, and strong software compatibility. However, the cost of both systems was too high, even after exploring university-supported discounts.

Fortunately, our internal investigation led to the discovery of a Biosemi ActiveTwo system housed within the university at the SOLO Labs. While it was not initially our first choice, the system aligned well with our experimental requirements. Biosemi's reputation for research-grade performance, active gel-based electrodes, and support for up to 256 channels made it a viable candidate. More importantly, the system was partially compatible with the synchronization architecture designed for this project.

As such, the Biosemi ActiveTwo was selected for all subsequent experimental recordings presented in this thesis.

Brand	Model	Wired	Wireless	Number of channels	Additional sensors supported	Intended Use
Advanced Brain Monitoring	B-Alert® X10	×	✓	9 channels	✓	Neuromarketi+G2:G41ng, BCI, identify biomarkers
	B-Alert X24	×	✓	20 channels	✓	
BIOPAC Systems Inc.	EEG100C	✓	×	16 channels	×	Epilepsy, tumor pathology, sleep studies, evoked responses,
						Cognition studies.
ANT Neuro	eegosports	×	✓	64 channels	✓	BCI, neurofeedback
						neurorehabilitation, neurogaming
Biosemi	ActiveTwo ×	✓	×	16-256 channels	✓	Electrophysiology research
Brain Products	actiCAP system	✓	×	8-256 channels	✓	Neuroscience
	ACTi- Hamp	✓	×		✓	neurofeedback
	Brain -Amp	✓	×		✓	neurophysiological
	Brain -Vision	✓	×		✓	
	V-amp	×	✓		✓	
	MOVE system	×	✓		✓	
Cognionics Inc.	HD-72 EEG	×	✓	64 channels	✓	Neurofeedback,
	Quick-20	×	✓	21 channels		neurodiagnostic
CompumedicsNeuroscan	Grael	✓	×	Up to 256 channels	✓	Clinical
	Nu-Amps	✓	×		✓	neuro-diagnostics,
	Syn-Amps	✓	×		✓	research
Emotiv	Emotiv EPOC	×	✓	5-14 channels	✓	Research, personal use
	Emotiv Insight	×	✓		✓	
g. Tec	g.BSamp	✓	×	Up to 256 channels	✓	BCI, neuroscience, neurotechnology
	g.Hiamp	✓	×		✓	
	g.USBamp	✓	×		✓	
	g.MOBIlab+®	×	✓		✓	
	g.Nautilus	×	✓		✓	
	Unicorn Hybrid Black	×	✓		✓	
Neuroelectric	Enobio 8	×	✓	8-32 channels	✓	Neuroscience, BCI, neurogaming,
	Enobio 32	×	✓		✓	Neurofeedback
	StarSim 8	×	✓		✓	
	StarSim R32	×	✓		✓	
NeuroBioLab	NBL640	✓	×	24 channels	×	Neurobiofeedback
OpenBCI	OpenBCI 32bit	×	✓	4-21 channels	✓	BCI, biosensing, neurofeedback
	Open BCI Cyton	×	✓		✓	
	OpenBCI Ganglion	×	✓		✓	
	Ultracortex BCI	×	✓		✓	
Narosky	Brainwave	×	✓	Single channel	✓	BCI, neurogaming, neurofeedback,
	Mind Flex	×	✓		✓	neuroscience, meditation
	Mind Wave	×	✓		✓	
	ThinkGearAM (TGAM)	×	✓		✓	
Medical Computer Systems	NVX52	✓	×	48 channels	✓	Research

Table 6.1: Comparison of EEG systems adapted from [Dai et al., 2023].

Motion Capture System

In parallel, we conducted a detailed investigation into MoCap platforms capable of synchronizing with neural recordings while supporting fine-grained limb tracking. Our goal was to identify a system that would provide sufficient spatial resolution, low latency, and adaptability to real-time conditions typical of motor control experiments.

We began by evaluating the ZeroKey Quantum RTLS, an ultrasonic-based real-time localization system known for sub-millimeter accuracy in industrial settings [ZeroKey Inc., 2023]. Its accuracy was impressive, but the system was clearly designed for industrial applications rather than human motion capture. It required a static environment, a grid of anchor nodes, and complex calibration procedures which made it impractical for our needs.

Next, we considered the Microsoft Kinect sensor, informed by its prior use in EEG-motor decoding studies Sosnik and Zheng [2021]. While affordable and easy to integrate, Kinect's accuracy drops significantly in occluded or fast-motion scenarios, which are common in upper-limb experiments. We also looked into AI-based markerless pose estimation tools like OpenPose, DeepLabCut, and Pose2Sim [Mathis et al., 2018, Pagnon et al., 2022]. These approaches promised scalable, low-cost tracking pipelines, but they also suffer from issues such as sensitivity to lighting, camera angle, and depth ambiguity.

As with the EEG search, we investigated possible alternatives at the university's labs. Although the explored MoCap systems outlined were promising, ultimately, the wearable inertial-based motion capture Movella Awinda system proved to be most suitable for our use case. It supports multi-limb tracking, provides real-time joint kinematics, and incorporates proprietary filtering and error correction algorithms to improve measurement reliability [Movella Inc., 2023a]. It is also partially compatible with available synchronization methods and offers advanced biomechanical analytics through the MVN software suite. Compared to other solutions, the Movella system offered the best trade-off between precision, flexibility, and integration, making it the most appropriate MoCap platform for this project.

As such, the Movella Awinda was selected as the motion capture apparatus for all subsequent recordings. Table 6.2 summarizes the comparative selection process of MoCap selection.

Table 6.2: Comparison of Evaluated Motion Capture Systems. **Credit: By Author**

System	Tracking Type	Precision / Accuracy	Biomechanical Modeling	Integration Complexity	Notes / Outcome
ZeroKey Quantum RTLS	Ultrasonic RTLS	Sub-mm	Not Human-Centric	High (Requires Anchors)	Designed for industrial assets; high cost; not practical for wearable use
Microsoft Kinect v1	RGB-D Camera	Moderate (low under occlusion)	Full-body Skeleton	Moderate (LSL-compatible)	Low cost, but limited accuracy under movement/occlusion
OpenPose / DeepLabCut / Pose2Sim	Markerless Vision (Deep Learning)	Variable (frame-dependent)	Inferred Joints Only	Post-processing Required	Susceptible to lighting/occlusion; not ideal for precise kinematics
Movella MTw Awinda	Inertial (IMUs)	High (proprietary filtering)	Real-Time Joint Kinematics	Seamless (MVN + Hardware Sync)	Available in lab; ideal balance between precision, mobility, and integration

Iterative Experiment Refinement

After hardware selection, the experiment design itself was subject to multiple iterations. We ran a series of pilot sessions with volunteer participants to troubleshoot timing, comfort, clarity of instructions, and overall workload. These iterations shaped both the technical implementation and the participant experience.

Stage I – Tracker Load and Sample Rate

The initial design aimed to record full upper-body kinematics for both left and right arms. However, early test sessions revealed that capturing bilateral motion with adequate trial numbers would significantly lengthen the experiment, resulting in participant fatigue and compromised data quality. Additionally, the Movella system's sampling rate was found to decrease with increased tracker count as shown in Table 6.3. These technical constraints and ergonomic limitations led us to explore simplified recording configurations. The final experiment employed five inertial trackers configured exclusively for the right arm, placed on: the hand, forearm, shoulder, scapula and sternum. This allowed a maximal motion capture sampling rate of 100 Hz and ensured coverage of the most relevant kinematic segments for decoding upper-limb motion.

Table 6.3: Movella MTw Awinda Wireless Update Rates by Tracker Count. **Credit: [Movella Inc., 2023a]**

Number of Trackers	Update Rate (Hz)
1–5	120
6–9	100
10	80
11–20	60

Stage II – Trial Timing and Cue Synchronization

Participants reported that the original trial pacing, adapted from Sosnik and Zheng [2021], felt rushed. This was especially true for imagined movement blocks. We experimented with several schemes, eventually settling on the following version. Each trial was expanded to five seconds: a 2.5-second reach phase followed by a 2.5-second return. Block durations were modified as follows: V-block (8s), P-block (5s), R-block (10s), IBI (30s). This scheme improved participants' ability to perceive cues and synchronize trial execution accordingly. A complete description of the experimental paradigm and illustrative diagrams are provided in Section 6.1.4.

Stage III – Visual Cue Integration

Relying on sound alone caused confusion in some early sessions. Participants occasionally missed the beeps or lost track of timing. We mitigated this issue by incorporating simple visual cues (e.g., directional arrows, highlighted targets) to reinforce the auditory signals. This multimodal cueing strategy was implemented such that Runs 1 and 3 presented both visual and auditory stimuli, while Runs 2 and 4 relied solely on auditory tones. Research indicates that visual cues can enhance brain responses during motor imagery tasks. For instance, [Kilmarx et al., 2024] found that imagining something right after seeing it (short-term visual imagery) creates more robust and decodable EEG patterns than trying to imagine it without any visual aid (from long-term memory). This supports the use of visual cues alongside auditory ones in BCI experiments.

Stage IV – Exploring Compositionality

Inspired by theories of compositional motor control (see Chapter 4), we introduced new movement targets and paths designed to investigate how participants mentally combine simple movements into more complex ones. Five spatial targets were defined: four corner positions and a central fifth target. In later runs, five dynamic trajectories were introduced, with the fifth trajectory designed as a linear combination of the first and fourth (see Figure 6.1).

Stage V – Reducing Fatigue

Even after making several improvements, long recording sessions still caused participants to feel tired and uncomfortable. As such, we experimented with longer rest breaks, mid-session pauses, and the option to split recordings across two days. We decided to let participants opt for whichever option was most suitable according to their constraints. They had the choice between mid-session pauses, or to split recordings across two days. These strategies helped reduce physical and mental strain while preserving data quality and participant motivation.

6.1.4 Experiment Design and Trial Structure

The experiment was designed to collect simultaneous recordings of brain activity and upper-limb motion, with the goal of investigating the neural correlates of both executed and imagined reaching movements. Each session lasted approximately 60 minutes and consisted of four runs. Each run alternated between executed and imagined movements and followed a consistent structure to ensure control and repeatability. Participants were sat comfortably in a chair with their dominant arm resting on a starting pad placed on the armrest. All stimuli, cues, and instructions were presented on a screen facing them, and pacing was reinforced through auditory tones.

Task Format and Targets

Each run included five blocks (labeled T1–T5), with each block targeting a specific movement target or trajectory. Each block contained 12 trials in which participants repeatedly moved (or imagined moving) toward the same target or along the same trajectory. Targets were either static (e.g., top-left, bottom-right) or dynamic (continuous paths like vertical or lateral sweeps). Each was represented by either a square or an arrow on the screen, depending on the movement type (see Figure 6.1).

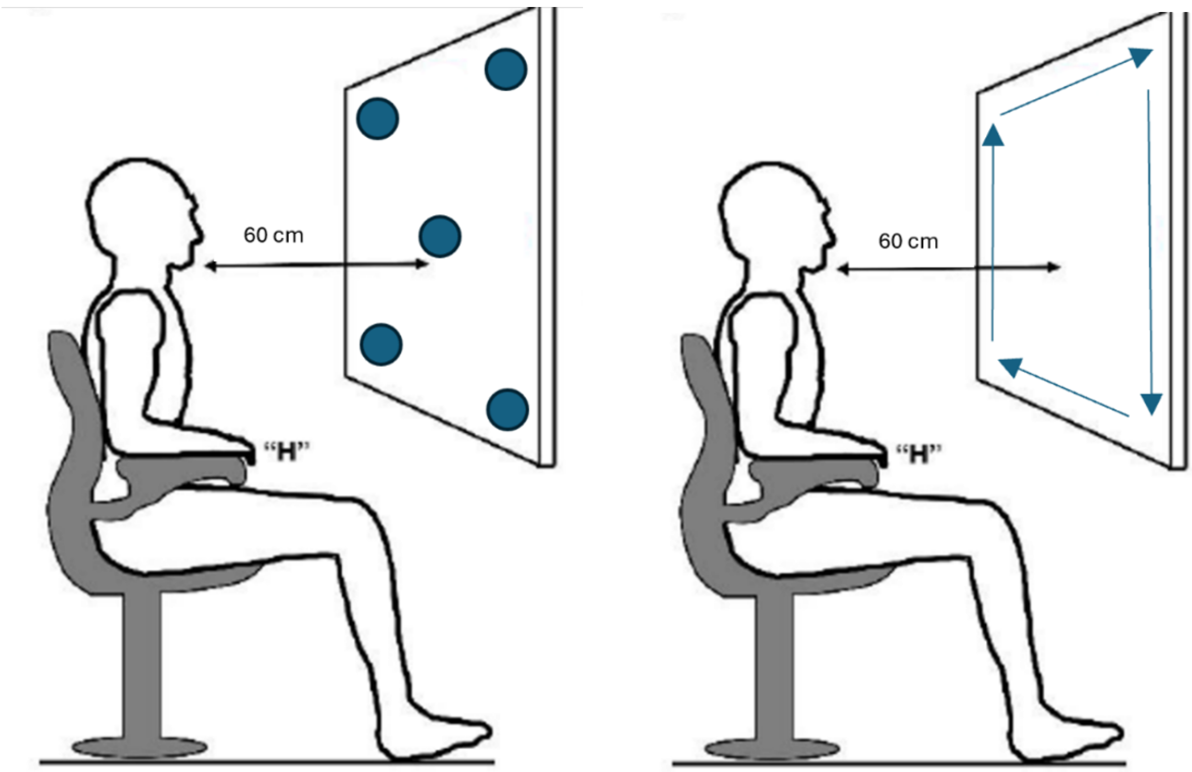

Figure 6.1: Visual layout of static targets (left) and trajectories (right). Targets are labeled from 1 to 5, starting from the top-left corner and proceeding clockwise; Target 5 corresponds to the central target shown on the left. Trajectories are similarly numbered 1 through 5. Notably, trajectory 5 combines trajectories 1 and 4 involving a horizontal sweep from left to right (Trajectory 1), followed by a vertical sweep from bottom to top (Trajectory 4) as illustrated on the right. *Credit: By Author, adapted from [Sosnik and Zheng, 2021].*

Trial Timing and Structure

Each individual trial lasted 5 seconds and was divided into three distinct phases:

- **Movement Initiation (0–2.5s):** A 4 kHz tone signaled the start of the trial. Participants reached (or imagined reaching) toward the displayed target. They were encouraged to pace their movement naturally, starting after the cue and progressing smoothly toward the goal.
- **Pause at Target (2.5s):** Until the midpoint of the trial, participants reached the target and briefly paused. This pause varied slightly depending on their pacing
- **Return to Start (2.5–5s):** A second tone at 2.5 seconds (6 kHz) signaled the participant to return to the home position, completing the trial by the 5-second mark.

This consistent timing structure ensured reliable synchronization across EEG and MoCap data streams and replicable trials. While the trial timing was externally constrained, the details of forward movement and pause duration varied slightly based on participant behavior. This design choice was adopted in light of the findings from Section 6.1.3

Instructional and Rest Blocks

Each block followed a repeating structure of instruction, preparation, execution/imagery, and rest:

- **Visual Message (V) Block:** A brief on-screen cue informed the participant of the upcoming task for a duration of 8 seconds (e.g., ”execute reach to target 2” or ”imagine sweeping motion along arrow”).
- **Preparation (P) Block:** The target or trajectory was visually presented for 5 seconds. Participants used this time to mentally prepare or rehearse the upcoming movement.
- **Trial Execution (T) Block:** Participants performed 12 trials based on the presented instruction and trajectory. Executed and imagined trials were split by the half-run point.
- **Rest (R) Block:** A 10 second rest period followed each execution/imagery block. Participants were asked to remain still and minimize any movement, talking, or clenching, though this was not strictly enforced. These segments were excluded during data processing.
- **Inter-Block Interval (IBI)** After each half-run (five blocks), participants were given a longer 30-second rest period. These intervals served as a reset period and as a baseline measurement for neural activity in a relaxed state. Participants were instructed to avoid swallowing, fidgeting, or jaw tension.

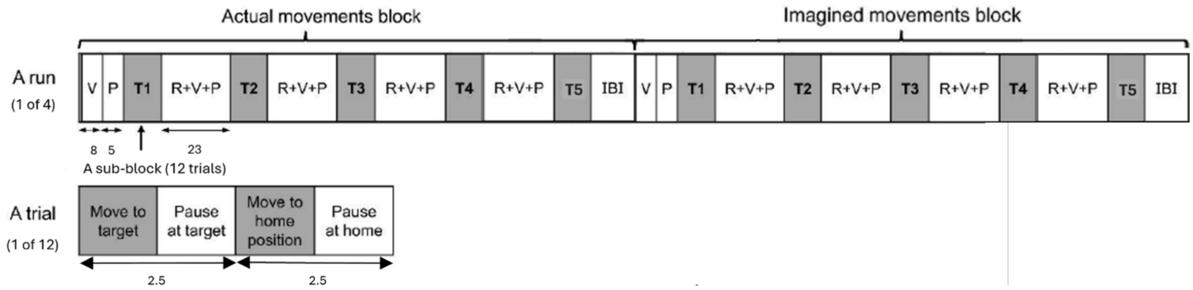

Figure 6.2: Overview of the timing structure for a full run. Each run includes blocks of visual instruction (V), preparation (P), trial execution (T), rest (R), and inter-block intervals (IBI), alternating between executed and imagined conditions. *Credit: By Author, adapted from [Sosnik and Zheng, 2021]*

Participant Instructions

Participants were provided with detailed instructions and real-time guidance during the session to ensure consistency across conditions. These measures aimed to support comparative analysis under highly controlled and repeatable circumstances. Specifically, participants were instructed to:

- Follow the auditory cues precisely to initiate and return during each trial, aiming for smooth, natural pacing.
- Keep their gaze fixed on the target or trajectory to minimize eye movement artifacts.
- Be wary of performing physical movement during imagined trials.
- Remain relaxed, upright, and silent during rest intervals.

6.1.5 Experimental Setup and Hardware Configuration

The experiment was conducted using a synchronized multimodal setup that enabled the simultaneous recording of EEG and MoCap data. This section describes the hardware components, how they were physically arranged, and the synchronization architecture that linked all parts of the system. The goal was to ensure a replicable infrastructure, minimal latency and, comfort for participants throughout the recording.

Recording Equipment

Neural activity was recorded non-invasively using a BioSemi ActiveTwo system (BioSemi B.V., Amsterdam, Netherlands) with a 32-channel electrode cap. Electrodes were placed according to the international 10–20 system (see Figure 5.2b). EEG signals were sampled at 1024 Hz, referenced using BioSemi's standard Common Mode Sense (CMS)/Driven Right Leg (DRL) electrode configuration. In addition, Electrooculogram (EOG) was recorded using four external electrodes sampled at 1024 Hz as well. Simultaneously, MoCap was achieved using the MVN Awinda system by Movella, which consists of 17 wireless MTw Awinda Inertial Measurement Units (IMUs). For the purposes of this study, only upper limb segments were used, specifically the shoulder, upper arm, forearm, and wrist totaling 5 wireless MTw trackers. Motion data was sampled at 100 Hz and included acceleration and orientation measurements.

Participant Seating and Physical Layout

Participants were seated in an adjustable office chair with armrests. A computer monitor was placed at eye level, 60 cm in front of the participant, to display instructions and stimuli (see Figure 6.3). The EEG cap was secured on the participant's scalp, with flat ribbon cables connecting it to the BioSemi A/D box behind the chair as illustrated in Figure 6.11. The motion capture sensors were worn over a soft, fitted MoCap suit. Care was taken to ensure participant comfort and minimize cable tension.

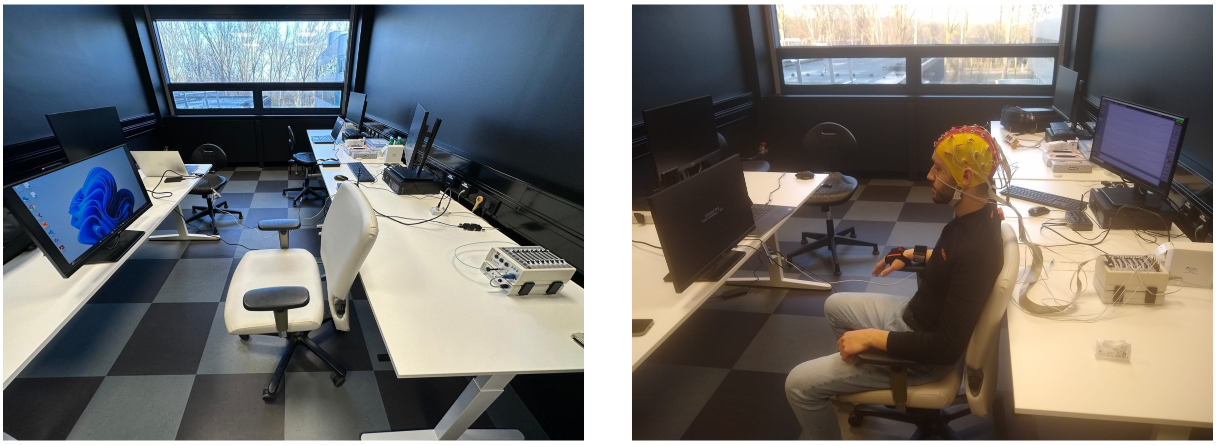

Figure 6.3: Overview of the lab seating arrangement, stimulus presentation, and hardware synchronization components. The participant is seated on the office chair using pre-defined measurements. The experimental task is presented on the monitor facing them, and the EEG cap was secured and connected to the AD box via flat ribbon cables behind them. *Credit: By Author*.

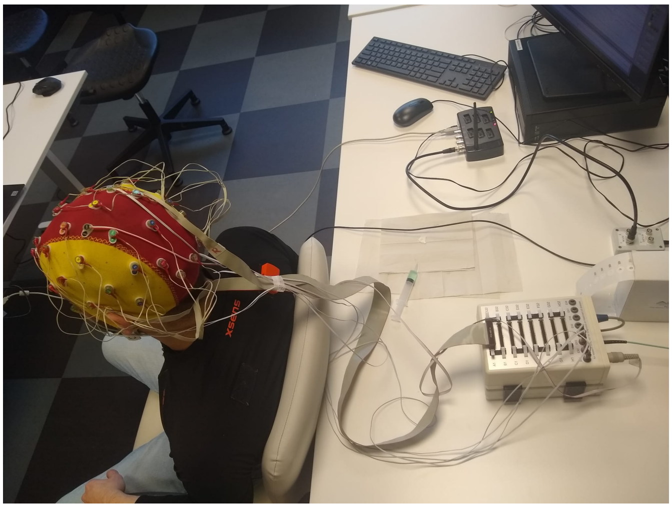

Figure 6.4: EEG cap secured and connected to the AD box via flat ribbon cables. *Credit: By Author*

System Architecture and Data Flow

To ensure that EEG, MoCap, and experiment triggers were all temporally aligned, a custom system architecture was implemented, as illustrated in Figure 6.5.

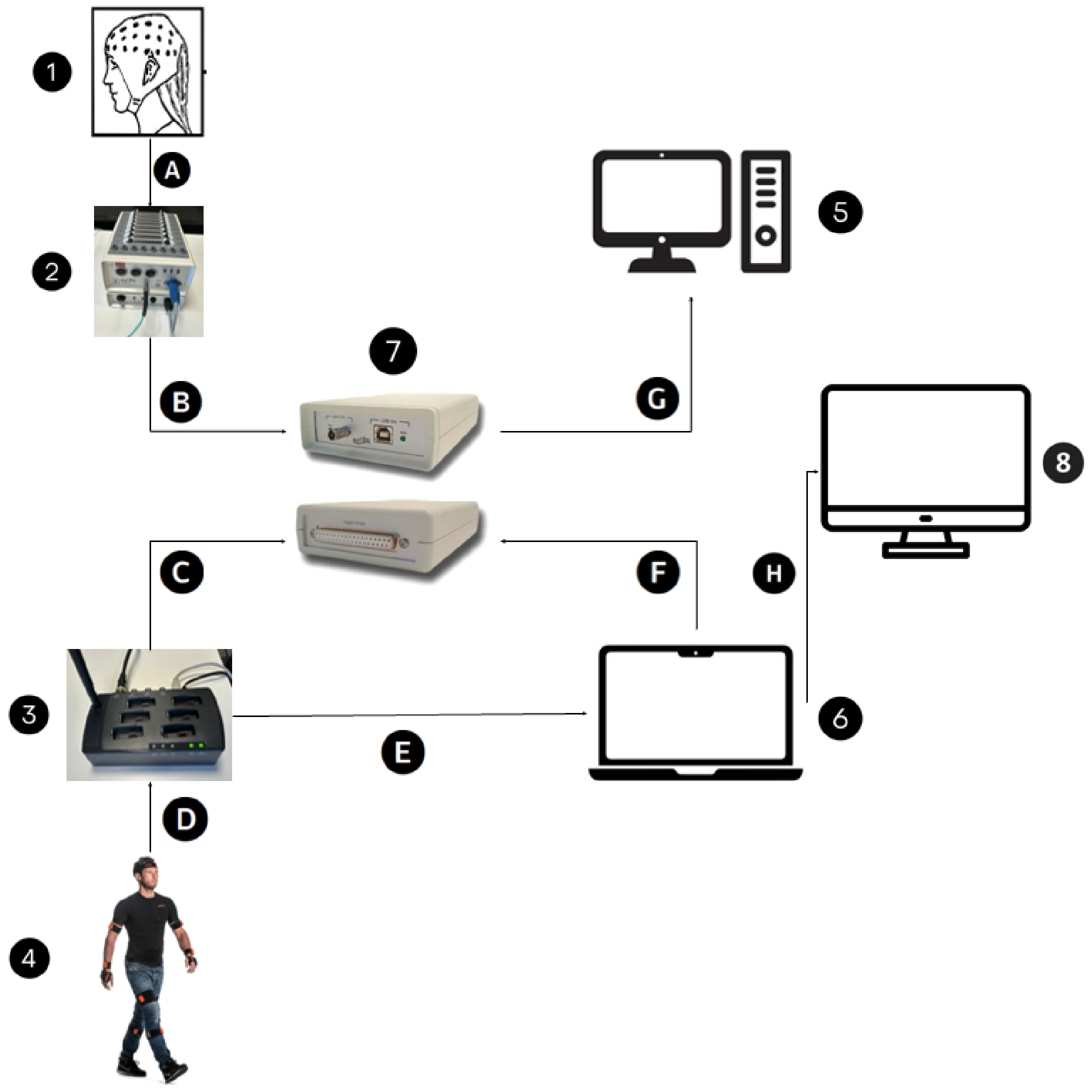

Figure 6.5: Overview of the hardware and connection layout used during the experiment. Numbers refer to components; letters refer to physical or logical connections. *Credit: By Author*

Components (Numbered): (1) Active electrode 32-channel EEG cap; (2) Mark II EEG A/D box ; (3) Movella Awinda Station; (4) Movella Motion Capture Suit with Inertial Trackers; (5) EEG Acquisition Desktop; (6) Personal Laptop; (7) Biosemi USB Receiver; (8) External Monitor.

Connections (Labeled A–G): A) Flat ribbon cables output from EEG cap to the A/D box; B) Optical cable output from A/D box to Biosemi USB receiver; C) BNC coaxial output from Awinda Station to Biosemi USB receiver via BNC Distribution Box; D) Wireless output from Inertial Trackers to Awinda Station; E) USB output from Awinda Station to personal laptop; F) Digital trigger from UsbParMarker to Biosemi USB receiver (via DB-25 to DC-37); G) USB output from Biosemi USB receiever to EEG desktop; H) HDMI output from laptop to external monitor. (C) & (F) Combined output from BNC Box to Biosemi 37-pin input;

Detailed Description of System Architecture

In this subsection, we provide the reader with a detailed description of all components and connections presented in Figure 6.5, explaining its function, physical location in the lab, and how it interacts with other components during data collection. The numbering and lettering used here correspond to the labels in the diagram for consistency and clarity.

Experiment Laptop:
A personal laptop (6) was used to run both the MT Manager software, responsible for controlling the Movella Awinda motion capture system, and PsychoPy, which executed the experimental protocol and managed stimulus presentation and timing.

EEG Acquisition System:
EEG data was recorded using a dedicated acquisition desktop (5) connected to a Biosemi ActiveTwo USB receiver (7) and A/D box (2). The system was controlled using Biosemi's ActiView software. The AD box interfaced (A) with the EEG cap (1) and the USB receiver (7) collected trigger signals via a shared 37-pin Sub-D connector (F), which allowed synchronized registration of experimental events.

Display Monitor for Participant:
An external monitor (8), connected via HDMI (H) to the experiment laptop (6), was positioned exactly 60 cm away from the armrest of the chair in which the participant was seated. The height of the screen's bottom bezel to the floor was such that it was 15 cm above the chair's armrest (see Figure 6.3). This screen was used to present the visual stimuli for each experimental block, ensuring the participant's view remained fixed and ergonomically comfortable.

Movella Awinda Station:
The motion capture system included the Awinda Station (3) hardware, which handled wireless communication (D) with the wearable inertial sensors (4). It also served as the master device for synchronization, sending TTL pulses via its BNC OUT port (C) at recording onset.

Synchronization and Cabling:
Trigger signals were routed through a custom-built cable interface involving a BNC distribution box, the UsbParMarker and a 37-pin Sub-D synchronization hub. This apparatus combined digital triggers from the experiment laptop (6) (via UsbParMarker and DB-25 to DC-37 parallel connection cable (F)) and synchronization pulses from the Awinda Station (3) into a shared output connected to the Biosemi USB receiver (7). This ensured aligned start times between EEG and MoCap recordings, as detailed in Section 7.1.1.

Software Infrastructure

Several programs ran in parallel across two machines to manage data collection:

- **PsychoPy**: Controlled the experimental task, stimulus display, and timing of event markers (laptop).
- **ActiView**: Captured and displayed incoming EEG signals and trigger events (EEG PC).
- **MT Manager**: Controlled the recording of inertial data from the motion sensors (laptop).
- **UsbParMarker:** A Python module used to send digital event triggers to the EEG system.

6.1.6 Middleware, Synchronization & Consistency Checks

Accurate synchronization between the EEG and MoCap systems was critical to ensure reliable data alignment for multimodal decoding. We explored both software-based and hardware-based synchronization approaches, ultimately developing a custom hardware solution that allowed for real-time alignment of recording streams.

Software-Based Synchronization via LSL

The first approach we investigated was software-based synchronization using the Lab Streaming Layer (LSL) framework. LSL is a widely adopted middleware developed for real-time acquisition and synchronization of time-series data from multiple devices. It uses a shared network clock to manage device-specific offsets and compensate for clock drift, allowing streams to be aligned during post-processing with sub-millisecond accuracy [Kothe, 2014]. LSL also supports the embedding of time-stamped event markers and provides tools such as LabRecorder and LSL Viewer for real-time diagnostics.

We were able to successfully stream EEG data from the Biosemi ActiveTwo system using Biosemi's native LSL plugin. This stream was visible and verifiable via LabRecorder. However, streaming motion data from the Movella Awinda system proved to be a challenge. Despite efforts using Movella's LSL plugin, the data stream was not detected.

To isolate the problem, we tested an alternative: a Microsoft Kinect sensor integrated via the open-source Kinect-LSL plugin. Skeletal motion data was successfully streamed and synchronized, confirming that LSL was functional on our end. This led us to investigate Movella's software and revealed that our system was running on the MVN Animate license, which does not support biomechanical data export or LSL-based streaming. These features require the higher-tier MVN Analyze license, which was not available under our university's license agreement.

Hardware-Based Synchronization via TTL Triggering

In parallel with these efforts, Movella had released documentation on hardware synchronization for third-party systems [Movella Inc., 2023c], including detailed instructions on synchronizing with ANT Neuro EEG systems via TTL pulses transmitted through BNC ports on the Awinda Station (see Figure 6.6a) [Movella Inc., 2023b]. These TTL triggers can be configured to start and stop events, using either rising or falling edges, specific pulse widths, and adjustable delays (illustrated in Figure 6.6b).

Although this guide was designed for ANT Neuro systems, a technical consultation with Movella's support team suggested that a similar approach could be applied to Biosemi's ActiveTwo system, which allows external triggers to be received via a USB interface coupled with an analog-to-digital conversion box. The main challenge layed in interfacing these two systems, as the Awinda Station outputs synchronization pulses via standard BNC coaxial cables, while the Biosemi system requires digital trigger input through its own USB-based receiver, which uses a proprietary format and voltage levels.

It is worth mentioning that even with the missing license, it was still possible to initiate synchronization by using MT Manager. This is Movella's software for configuring and recording data from the Awinda system. Unlike MVN Animate and MVN Analyze, which offer real-time visualization and biomechanical output, MT Manager focuses on device management and raw data acquisition [Inc., 2014].

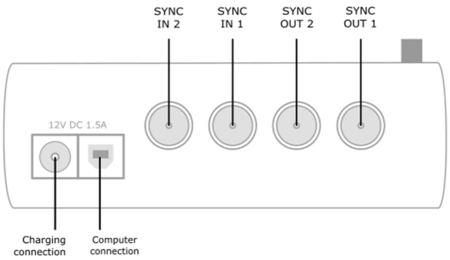

(a) The Xsens Awinda Station BNC connectors, two Sync IN and two Sync OUT. *Credit: [Movella Inc., 2023b]*

(b) Polarity: Rising/ falling edge (Sync IN) or positive/ negative pulse (Sync OUT). *Credit: [Movella Inc., 2023b]*

Figure 6.6: Awinda Station synchronization BNC ports (left) and pulse polarity of TTL trigger (right).

Custom Cabling and Logging Setup

To mitigate these incompatibilities, we collaborated with university lab technicians to develop a custom hardware interface capable of delivering synchronization and digital trigger signals simultaneously. The solution included the following components:

- **BNC OUT from Awinda Station:** Configured as the synchronization master, the Awinda Station sends a TTL pulse from its BNC OUT port (illustrated in Figure 6.6a) as soon as recording begins in MT Manager software.
- **BNC Distribution Box:** A custom-built passive box containing four BNC ports (two IN, two OUT) used to split and route the synchronization pulse (see Figure 6.7).
- **UsbParMarker:** Another cable, originating from the experiment laptop, allows digital event codes (e.g., run starts, trial blocks, etc.) to be sent using a USB-to-parallel cable connector known as UsbParMarker (see Figure 6.8a). It is a replacement for the parallel port (of type DB-25), also known as Line Printer Terminal (LPT) which was built by the university labs as most laptops nowadays are devoid of parallel ports. This cable interfaces with a DB-25 to DC-37 parallel connection cable (see Figure 6.7).
- **Convergence Hub:** Both the synchronization pulse (from the Awinda Station to the BNC distribution box) and the digital trigger signals (from the laptop via the UsbParMarker through a DB-25 to DC-37 parallel cable) are routed (see Figure 6.7) to a shared 37-pin Sub-D output interface (see Figure 6.8b). This shared interface connects directly to the Biosemi USB receiver and analog/digital converter (see Figure 6.9), allowing both types of signals to be registered as digital triggers in the EEG data stream.

This configuration allowed for both global synchronization and event marking to be injected into the EEG stream through a single, converged hardware pathway. The entire setup is was first illustrated in Section 6.1.5.

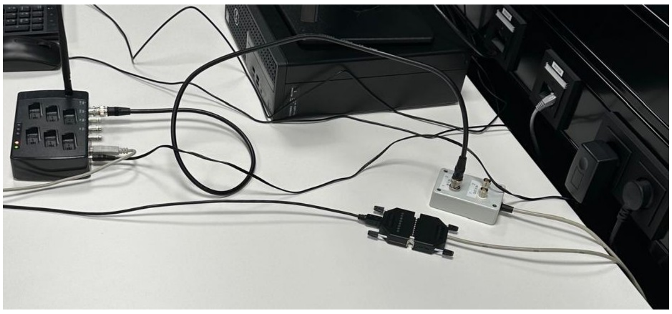

Figure 6.7: Xsens Awinda Station (left: black box), BNC Distribution Box (middle: white box), and UsbParMarker + DB-25 to DC-37 parallel cable (right: junction). *Credit: By Author*

(a) UsbParMarker. *Credit: [SOLO Labs]*

(b) 37 pins male Sub-D parallel connector. *Credit: [B.V.]*

Figure 6.8: UsbParMarker (left) and 37 pins male Sub-D parallel connector (right).

Figure 6.9: Biosemi analog/digital converter 37 pins male Sub-D parallel port. *Credit: [Movella Inc., 2023c]*

6.1.7 Data Pipeline – From Raw Signals to Labeled Dataset

To ensure a reproducible and scalable preprocessing workflow, we designed a modular pipeline that transforms raw data EEG and MoCap data into a structured and preprocessed dataset with consistent formatting and metadata.

Data Pipeline Workflow

The goal of the pipeline is to convert raw multimodal recordings into an organized format suitable for machine learning. This includes aligning the EEG and motion streams, segmenting trials based on event markers, associating relevant metadata with each segment, and exporting everything into a compact, hierarchical format for downstream processing. As such, the pipeline was designed with the following principles in mind:

- **Modularity**: Each component handles a single modality or task (e.g., EEG cleaning, motion integration, trial segmentation).
- **Reusability**: Script configurations are defined separately to enable adaptation across different recording sessions or datasets.
- **Precision and Metadata**: Trial segmentation is informed by precise EEG triggers, enabling each trial to carry detailed labels such as run number, repetition count, target ID, execution type, and trial phase.
- **Compatibility**: Output is saved in a structured `.h5` format, facilitating integration with machine learning libraries and possibly real-time applications.

The entire preprocessing pipeline is controlled through a master script (`pipeline_full.py`) which calls several modular components responsible for signal preprocessing, alignment, segmentation, and export. A simplified overview of the pipeline is shown in Figure 6.10.

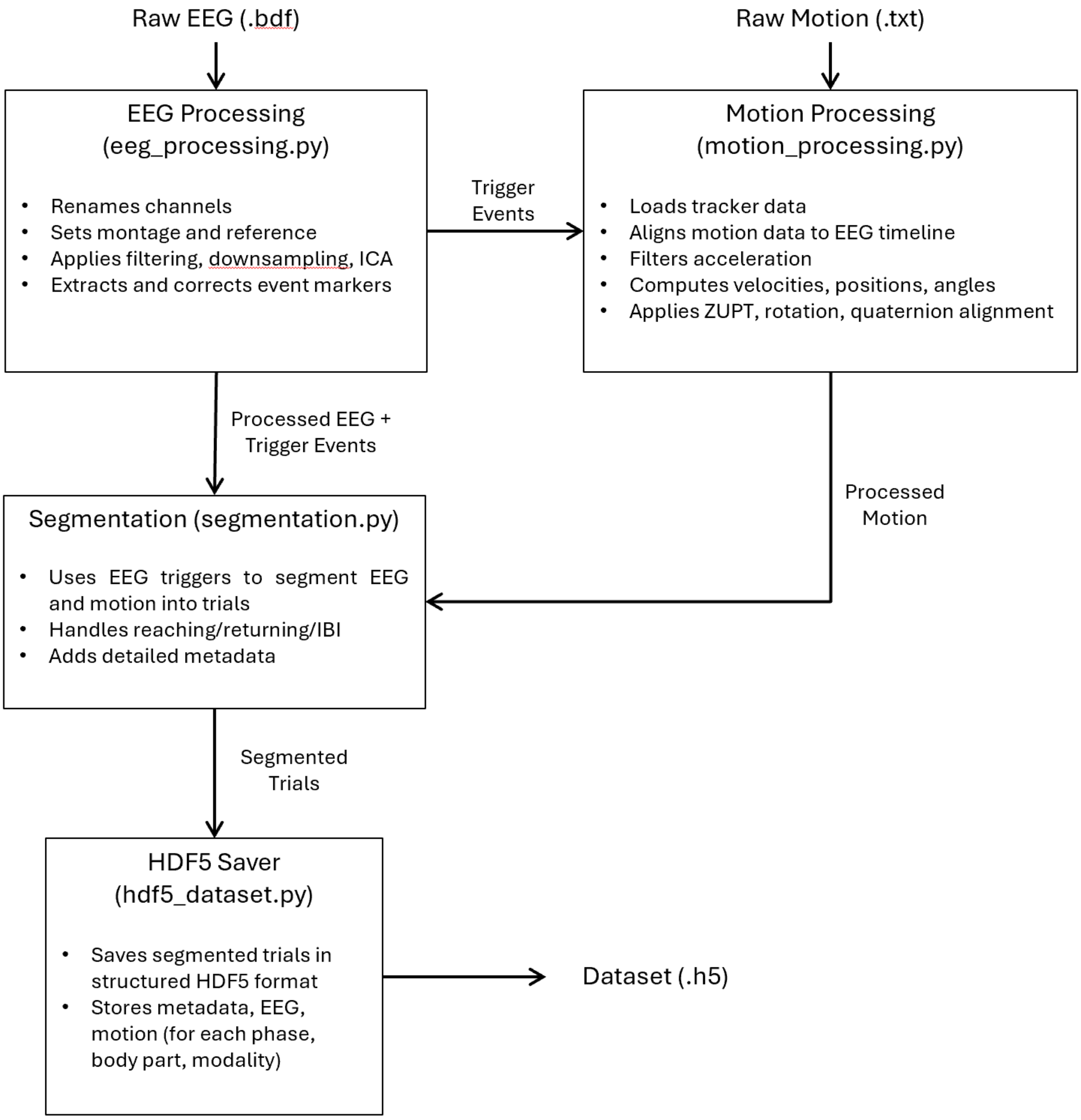

Figure 6.10: Flowchart of the preprocessing pipeline. Raw EEG and motion data are handled by dedicated scripts for preprocessing and alignment, followed by segmentation into labeled trials and saving to an HDF5 dataset. Each module is designed to be reusable, configurable, and extendable for future experiments. *Credit: By Author*

EEG & Motion Data Pre-processing

Prior to trial segmentation and conversion into a structured dataset, raw EEG and MoCap recordings underwent a series of preprocessing steps aimed at removing artifacts and preparing the data for further analysis. While minimal preprocessing was applied overall, specific cleaning steps were used to mitigate known issues.

EEG Data

EEG signals are highly sensitive to noise. However, given the recent success of deep learning models in extracting high-level features directly from raw or minimally processed EEG data [Pancholi et al., 2022], we followed a minimal preprocessing strategy. The preprocessing pipeline can be summarized by the following steps:

- **Loading and renaming channels** by reading raw EEG files using MNE-Python. Channels were renamed and reordered according to the standard 10–20 system.

- **Notch filtering** at 50 Hz to remove powerline noise.
- **Bandpass filtering** in the 0.1–40 Hz range to isolate relevant motor-related brain activity.
- **Re-referencing** the EEG signal to reduce channel-specific bias.
- **Artifact correction** by applying ICA to remove blink, muscle, or cardiac artifacts. EOG channels were used to help identify and reject artifact components.
- **Event detection and epoching** by parsing trigger channels to extract event markers. EEG signals were segmented into epochs aligned with task events (e.g., movement onset, return phase).

All preprocessing was logged, and intermediate outputs could be inspected visually using MNE and matplotlib plotting functions. A visual comparison of raw and cleaned EEG is provided in Section 7.1.2

Kinematic Data

In contrast, motion data which was captured via inertial sensors, presented more of a challenge. Unlike EEG, MoCap systems typically rely on proprietary algorithms to produce accurate position or velocity estimates. However, due to licensing restrictions, we only had access to raw IMU data, such as orientation and acceleration. As such, we were required to develop a custom pipeline to approximate these values. The preprocessing pipeline can be summarized by the following steps:

- **Coordinate alignment** by transforming IMU orientation data into a participant-centered coordinate frame to standardize movement direction across sessions.
- **High-pass filtering** (cutoff: 0.3 Hz) to remove low-frequency drift and gravitational bias;
- **Low-pass filtering** (cutoff: 12 Hz) to smooth out high-frequency sensor noise;
- **Baseline subtraction** using preparation and imagined rest phases;
- **Kalman filtering** to reduce noise in velocity and position estimates;
- **Zero Velocity Updates (ZUPT)** to suppress drift during assumed stable periods;
- **Integration methods** using both cumulative summation and the trapezoidal rule for velocity and position estimation.
- **Feature extraction** into estimated linear velocity, joint positions, and joint angles derived from quaternion chains (shoulder to hand).

Despite the various processing steps, the motion data still suffered from drift and growing inaccuracies over time, especially during the later parts of the recordings. We elaborate on the results in Section 7.1.2.

Segmentation and Trial Labeling

The preprocessed EEG and MoCap data were segmented into consistent and labeled epochs. Each trial was marked using digital triggers inserted during the experiment, with the following logic:

- **Start-of-Run Triggers:** Unique digital markers indicated the start of each run, encoding both the run number and task type (executed vs. imagined).
- **Block Labels:** Trials were grouped by block (T1–T5), with labels corresponding to target position or movement type.
- **Rest, Preparation, and IBI:** These segments were also segmented and labeled. Although not used for decoding, they served as baselines.

The segmented trials were stored in an HDF5 format, where each trial was saved as a separate data object, along with associated metadata (e.g., trial ID, label, condition, block number, task type). A separate inspection script was used to verify the consistency of the stored dataset, which is further described in Section 7.1.2.

Additional Processing Considerations

IBIs were treated as baseline segments and handled accordingly during preprocessing. Motion parameters during these intervals were explicitly zeroed out, as no movement was expected. In contrast, EEG data during IBIs was preserved to serve as a reference point for baseline brain activity. This design choice facilitates the model's ability to distinguish rest, preparation, and active movement states during both executed and imagined trials.

Furthermore, in order to provide ground-truth labels for imagined movement trials, an average motion profile was computed for each condition from the executed trials. This averaging process grouped executed trials by target and movement direction, computed the mean across matched trials, and assigned the resulting trajectory as ground truth for corresponding imagined trials. This approach relies on the idea that when someone repeats the same movement toward a target, they tend to follow a similar path. We use that pattern to estimate what the person likely intended to do during imagined movements, even though there's no actual motion data available.

The resulting dataset thus includes both real and imagined movement trials with temporally aligned EEG and motion features, each appropriately preprocessed and labeled to facilitate downstream modeling tasks.

6.2 Part B: Theoretical Approach – Modeling Internal Motor Representations

Following the challenges encountered in Part A, as outlined in Section 7.1.3, Part B of this thesis reflects a shift in modeling approach. This transition was not only a reaction to practical issues, but also an active decision informed by theoretical developments that occurred throughout the literature review process.

6.2.1 Rationale for Modeling Shift

Initial efforts in Part A explored end-to-end deep learning models, such as hybrid CNN-LSTM and transformer architectures, to decode 3D hand trajectories from EEG signals. These models were selected based on their demonstrated success in prior work [Pancholi et al., 2022, Wang et al., 2023c] and theoretical insights [Yoshimura et al., 2017]. As such, the pipeline was built accordingly. However, two key developments prompted a shift:

- **Empirical Limitations:** The experimental data collected for this thesis suffered from excessive noise. Despite rigorous preprocessing efforts, cumulative errors caused the motion data (velocity and position) unusable for accurate decoding. As a result, the collected dataset could not be used to train or evaluate decoding models reliably.
- **Theoretical Refinement:** During the literature review, it became increasingly clear that effective motor decoding may benefit from structured representations that align with how the brain internally encodes movement. Neural manifolds, movement primitives, and reference frame transformations pointed toward a latent space approach that emphasizes internal geometry and compositional abstraction over direct prediction of output coordinates.

6.2.2 Theoretical Foundations

The theoretical basis of this new modeling direction was drawn from a set of interconnected neuroscience principles that describe how movement may be represented in the brain as outlined in Chapter 4, but can be briefly summarized as follows:

- **Compositionality:** Instead of treating each movement as a unique signal, the brain may generate actions by adaptively combining smaller, reusable components or primitives. This makes movement both generalizable and efficient. The DMP framework provides a concrete mathematical model for this idea [Hotson et al., 2016]
- **Neural Geometry:** Motor planning and execution unravel within low-dimensional spaces, coined 'neural manifolds', that capture shared structure across tasks and trials [Chung and Abbott, 2021]. These manifolds organize neural activity into smooth, interpretable trajectories and support generalization across movement types and tasks.
- **Reference Frame Flexibility:** Spatial encoding in the brain is not fixed; it dynamically transforms between egocentric and allocentric reference frames [Herweg and Kahana, 2018, Ottenhoff et al., 2025]. Effective models must accommodate these internal dynamic shifts.

- **Latent Dynamics:** Instead of directly decoding EEG into Cartesian coordinates, we aim to model how neural activity evolves over time. The MARBLE framework does this by embedding neural activity samples into a latent space where the dynamics of said activity unravel as interpretable ’flow fields’ [Gosztolai et al., 2025].

6.2.3 Model of Choice: MARBLE

MARBLE is a neural manifold learning framework. It uses contrastive learning to embed neural samples into a latent space, where it learns temporal transitions between them as continuous vector fields (flow fields). The advantage of this approach lies in its unsupervised nature. It learns to organize neural representations based on their dynamics, clustering together similar movement intentions, even across different sessions or individuals. While MARBLE was designed for intracranial recordings, similar geometric principles have recently been adapted to EEG via models like GREEN [Paillard et al., 2024], motivating our attempt to explore MARBLE in the context of EEG-based decoding.

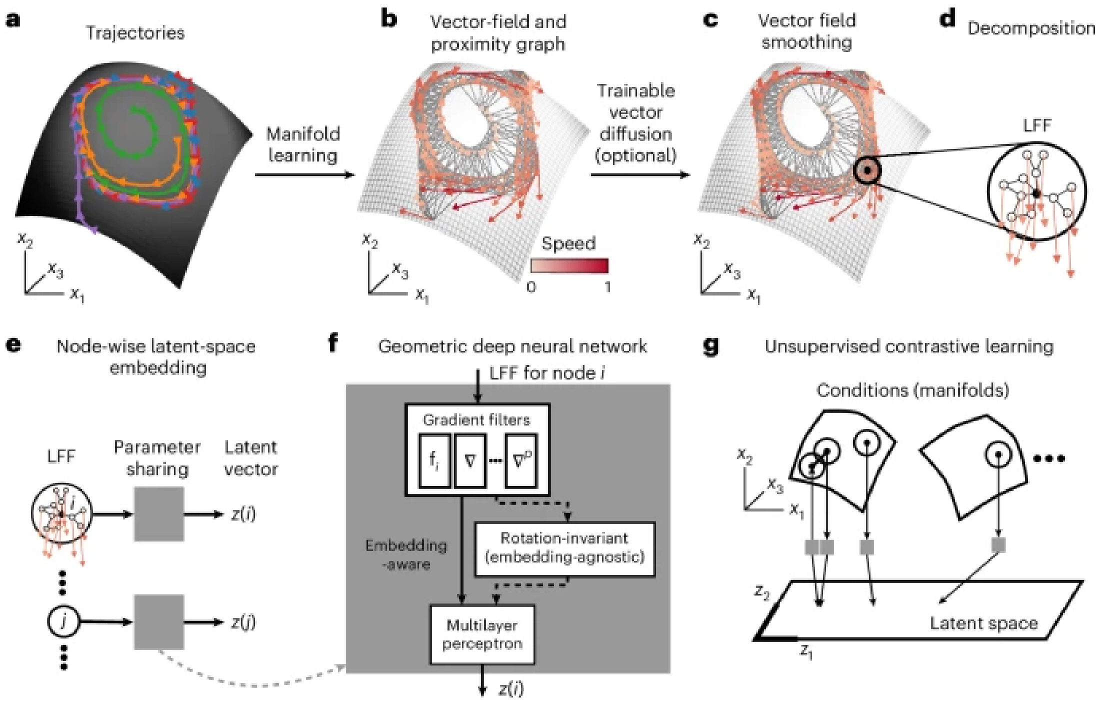

Figure 6.11: Overview of the MARBLE architecture, illustrating its key components and unsupervised manifold learning process. *Credit: By [Gosztolai et al., 2025]*

6.2.4 Public Dataset: WAY-EEG-GAL

Due to the unsuitability of our collected dataset, we opted to use the WAY-EEG-GAL public EEG dataset [Luciw et al., 2014], for preliminary experimentation. This dataset, previously used by Pancholi et al. [2022], includes EEG recordings from participants performing reaching and grasping movements in a 3D workspace.

The WAY-EEG-GAL dataset was designed to investigate the relationship between neural activity and natural upper-limb movements. It contains data from 12 healthy, right-handed participants who repeatedly performed a structured grasp-and-lift task using their right hand. Each trial consisted of the following sequence: reaching for an electro-magnet, grasping and lifting it off a surface, holding it momentarily, and then lowering it back to its original position. Trials were initiated and terminated via an LED cue. Variations in object weight and surface texture were introduced across trials to elicit different motor responses. Each participant completed up to 294 trials, resulting in a rich and diverse dataset suitable for decoding experiments.

Brain activity was recorded using a 32-channel EEG cap arranged according to the international 10–20 system and sampled at 512 Hz. Hand kinematics were captured using a 3D motion tracking sensor placed on the wrist. This sensor provided spatial coordinates of the hand throughout the movement sequence.

6.2.5 Reference Dataset: Macaque Reaching Task from MARBLE

To evaluate the MARBLE framework, [Gosztolai et al., 2025] re-analyzed an existing dataset involving a macaque monkey performing a center-out reaching task. In this experiment, the monkey was trained to move a handle from a central start position to one of seven target locations evenly spaced in a circle around it. These reaches were performed in response to a go cue, and each trial was associated with one of the seven spatial directions. Neural activity was recorded from the premotor cortex using a 24-channel implanted microelectrode array across 44 different sessions. Alongside this neural data, precise hand kinematics were captured using a robotic manipulandum equipped with motion sensors, providing continuous ground truth trajectories for each reach direction. The analysis focused on the neural signals immediately following the go cue, corresponding to the active movement phase.

When applied in an unsupervised fashion, MARBLE successfully reconstructed both the temporal structure of individual reaches and the global geometric layout of the task space. These findings served as a benchmark for adapting MARBLE for EEG-based decoding on the WAY-EEG-GAL dataset.

6.2.6 Analysis of MARBLE

This section outlines a series of explorations and experiments conducted during the second phase of the thesis, which shifted focus from direct regression models to a latent manifold-based approach. Due to the limitations of the collected dataset, the experiments focused on adapting the MARBLE framework for our purposes by employing its original intracranial dataset and the public WAY-EEG-GAL dataset [Luciw et al., 2014]. The first two replication tasks made use of MARBLE's public Github repository [1].

Replicating Latent Flow Fields with MARBLE

The first step involved running MARBLE's code and reproducing its built-in toy datasets and synthetic examples. These experiments helped clarify the model's architecture, loss functions, and training dynamics. In particular, we examined how the model constructs latent trajectories using contrastive learning, and how flow fields evolve over time to capture the internal structure of neural sequences.

In the specific example of vector fields on a flat surface, we defined four simple 2D vector fields with distinct underlying dynamics: two linear fields and two vortices. These served as test signals to evaluate how MARBLE encodes and organizes dynamic patterns in latent space.

[1] https://github.com/Dynamics-of-Neural-Systems-Lab/MARBLE/tree/main

- **Linear Left and Right**: These fields maintained constant vector directions throughout space.
- **Vortex Left and Right**: These mimicked rotational dynamics, producing curved motion patterns.

After feeding these into the MARBLE pipeline, the model used contrastive temporal learning to embed each trajectory into a 2D latent space. The goal was to see if the model could recognize patterns that change over time in a meaningful way and group similar ones together, while also telling apart different types of movement dynamics. Results are reported in Section 7.2.1.

Replicating the Monkey Reaching Task with MARBLE

This experiment replicated the end-to-end MARBLE pipeline on a dataset of intracranial recordings from macaque monkeys performing a center-out reaching task. The aim was to evaluate how MARBLE infers low-dimensional latent dynamics from neural activity and how these representations capture meaningful motor structure. The original dataset and preprocessed neural activity were provided via the MARBLE GitHub repository.

We ran the full MARBLE training pipeline, reproduced the original latent dynamics and classification metrics, and visualized the latent space evolution across different target conditions. This process provided valuable insight into how motor intention is organized in a low-dimensional manifold and how MARBLE learns to separate and interpolate across movement directions.

The process was divided into three main stages: data conversion, latent manifold construction using MARBLE, and subsequent visualization and decoding. Results are reported in Section 7.2.2.

Data Preparation

The original macaque dataset provided neural spiking data (in MATLAB format) recorded across multiple sessions and reach directions. To use this data with MARBLE, it had to be transformed into instantaneous firing rates suitable for modeling.

- The script *convert_spikes_to_firing_rates.py* was used to transform spike trains into smooth instantaneous firing rates via Gaussian convolution (using the Elephant toolbox).
- The data was binned at 20 ms resolution and stored as trial-wise tensors (*Trials* $\times$ *Channels* $\times$ *Time*).
- Only valid trials (non-empty, well-aligned) were included. Associated kinematic metadata (e.g., target direction and hand velocity) was extracted for downstream decoding.

Latent Space Construction

The next stage involved running the MARBLE training pipeline using the `run_marble.py` script:

- PCA was first applied per session to reduce dimensionality of the firing rate signals.
- Instantaneous velocity vectors were computed between time steps and paired with anchor embeddings.

- MARBLE used contrastive learning to associate each anchor with its future velocity, thus constructing a latent space structured temporally .
- Model-specific hyperparameters such as embedding dimension, kernel radius, and MLP architecture were configured as per Github documentation.
- The resulting embeddings and latent flow fields were saved in serialized `.pkl` files for visualization and decoding.

Analysis & Visualization

Finally, the latent representations were explored and used for decoding:

- The latent embeddings were visualized using PCA and UMAP to assess clustering by reach direction across trials.
- A decoder was trained to predict 2D hand position and from the latent features.

Preparing WAY-EEG-GAL for MARBLE

The following steps focused on preparing the WAY-EEG-GAL dataset so it could be used with the MARBLE framework. The aim was to take raw EEG and MoCap data and convert it into a clean, trial-by-trial format that MARBLE could work with. To do this, we built a step-by-step processing pipeline, where each stage handled a specific part of the data transformation. Results are reported in Section 7.2.3.

Raw Data Extraction

Raw participant recordings, originally stored in compressed archives (e.g., `P1.zip`), were extracted into a standardized directory structure using `extract_zipped_data_V0.py`. Each participant's data was stored as MATLAB `.mat` files in a `data/extract/sub-XX/raw/` hierarchy.

Metadata Loading and Alignment

Trial markers and behavioral metadata were preprocessed from a structured pickle file containing the AllLifts dataset using the `load_alllifts()` function. This enabled fast access to LED onset, movement initiation, and lift completion times, eliminating the need to repeatedly parse MATLAB structures.

Signal Preprocessing

Data preprocessing was applied to EEG and MoCap data using `data_preprocessing_V0.py`. Major steps included:

- **Downsampling:** EEG data was downsampled from 500 Hz to 100 Hz using zero-phase decimation.
- **Trial Cropping:** EEG signals were cropped to 2 seconds after LED onset; motion signals to 2 seconds after movement start.
- **Bandpass Filtering:** *Delta*, *Alpha*, *Beta*, *Gamma*, and total broadband signals were extracted using zero-lag Butterworth filters.
- **Referencing & Normalization:** Common average referencing and z-score normalization were applied.

- **Motion Scaling:** Kinematic channels were min–max normalized per condition.
- **Bad Trial Rejection:** Trials with response-times to stimulus onset exceeding an established threshold or strong artifacts using were discared using `reject_bad_trials()` as per [Pancholi et al., 2022].
- **Conversion to Rate-Like Representations:** EEG signals were converted into non-overlapping 20 ms windows of binned neural activity using `convert_to_rates_V0.py`. Output data was saved as `eeg_rate_data_gamma_20ms.pkl`.
- **Dimensionality Reduction via PCA:** Savitzky-Golay filtering (window=9, order=2) was used to smooth each trial, which were then stacked into a single matrix and passed through `fit_pca()` to extract components.

Each trial was stored as a dictionary containing raw EEG, band-filtered preprocessed EEG, preprocessed MoCap data, and trial metadata (e.g., labels, timings).

Running MARBLE with WAY-EEG-GAL dataset

To explore the compatibility of manifold learning with EEG-based decoding, we conducted a series of early experiments using the WAY-EEG-GAL dataset. We explored a range of hyperparameter configurations to identify suitable model setups. Key parameters included:

- **Manifold dimensionality:** [3, 5, 8, 10, 16]
- **Encoder depth:** [1, 2, 3]
- **Nodes per layer:** [16, 32, 64, 128]
- **Vector diffusion:** Enabled / Disabled
- **Momentum coefficient:** [0.90–0.95]
- **Dropout rate:** [0.1–0.3]

Embeddings were generated for each configuration to visually assess the latent structure of neural dynamics and to evaluate clustering patterns across movement conditions.

These early attempts were intentionally exploratory, with minimal model-specific tuning, and are reflected upon in Section 7.2.3.

6.2.7 Alternative Models Considered

Before shifting to MARBLE, we explored a range of model architectures for decoding movement trajectories directly from EEG data. These models varied in their theoretical basis, neural decoding strategy, and data requirements. We present an overview of these models below for the sake of completeness:

- **CNN-LSTM:** Served as initial baseline due to its strong performance in decoding 3D hand movements from EEG Pancholi et al. [2022].
- **Transformers:** Considered due to their strength in capturing long-range dependencies and self-attention mechanism but requires large dataset Wang et al. [2023c].

- **Riemannian Classifiers:** Considered due to their ability in exploiting geometric structure of EEG data. However, most implementations are tuned towards discrete classification rather than continuous decoding [Paillard et al., 2024].

- **Foundation Models (BrainBERT, Brant, LaBraM, MOMENT):** Considered due to the high-volume data it was trained on and strong results. However, built for high-resolution or intracranial recordings and not optimized for continuous decoding [Wang et al., 2023a, Zhang et al., 2023, Jiang et al., 2024, Goswami et al., 2024].

While each of these models offered attractive features, they shared a common limitation: they required either high-resolution data (as in intracranial recordings) or large quantities of it. Our collected dataset, due to its limitations, could not be employed for such approaches. Moreover, as our theoretical understanding of motor intention deepened, we moved away from models focused purely on raw input-output mappings.

6.2.8 Looking Ahead: Returning to Our Own Data

Once new EEG and motion data are collected using the improved pipeline described in Part A, the MARBLE-based decoding strategy will then be applied to it. The current analyses using public data are intended to validate the model choice and theoretical insights, with the goal of transferring the implementation to our own recordings.

Chapter 7

Results

7.1 Part A: Experimental Approach – End-to-End Deep Learning for Motion Decoding:

7.1.1 Middleware, Synchronization & Consistency Checks: Outcome.

After implementing the custom hardware-based synchronization setup described in Section 6.1.6, we performed a several steps to validate the alignment between the EEG and MoCap data streams. Initially, we suspected a temporal misalignment between EEG event markers and motion onsets. Specifically, trigger events in the EEG stream appeared to occur slightly after movement had already begun, as observed in raw motion recordings (see Figure 7.1). This prompted further investigation into possible causes such as packet loss, sending/receiving delay, or sampling rate inconsistency.

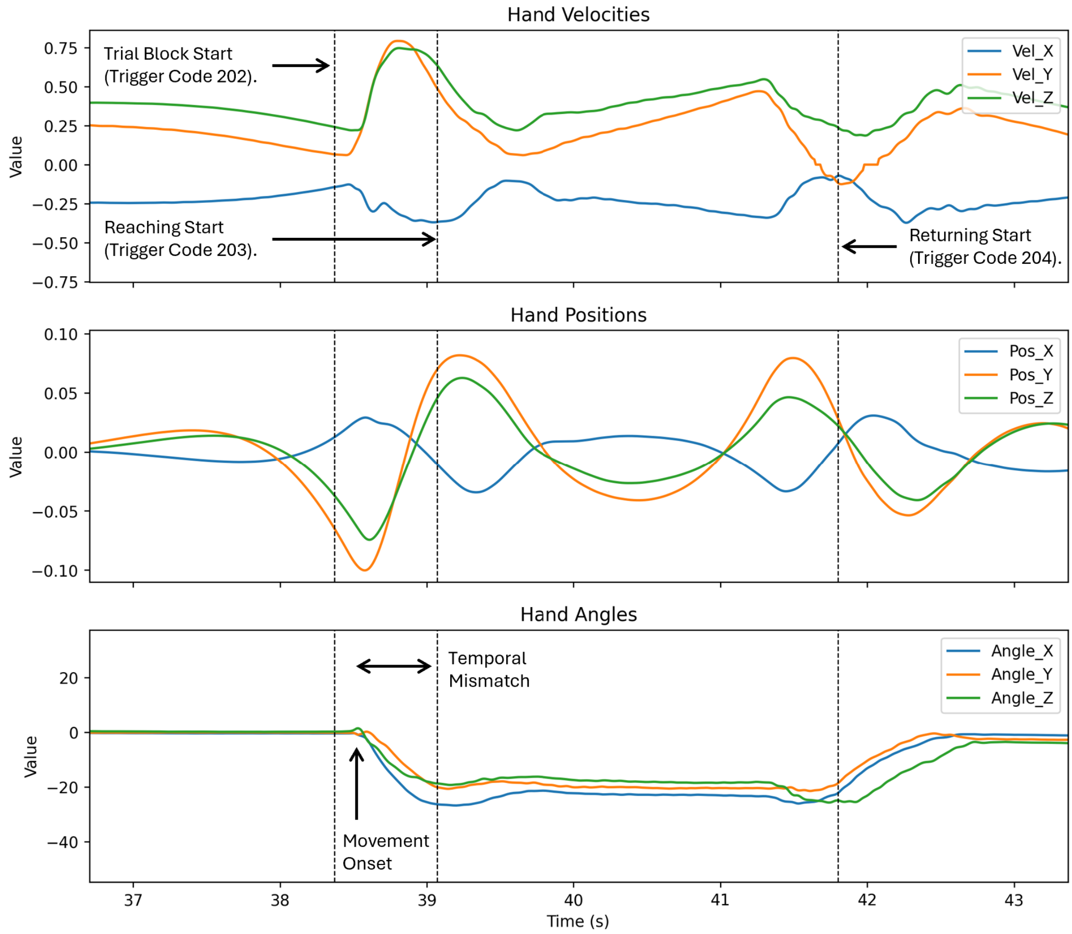

Figure 7.1: Example of motion data from a single trial illustrating a suspected trigger misalignment. Each subplot corresponds to a different modality recorded from the right hand: velocity (top), position (middle), and joint angle (bottom). The black dashed lines represent the EEG event triggers signaling the different stages of the trial. Notably, a visible delay is observed between the trigger position and the actual onset of movement, which should occur shortly after the cue. *Credit: By Author*

Stage I - Packet Loss

First, we considered packet loss in the motion data stream as a possible cause. Using a Python script, we analyzed the packet counters embedded in the raw motion files as illustrated in Figure 7.2. These counters are expected to increase sequentially for each recorded frame. By comparing the expected range of packets to the actual sequence, we verified that no packets were missing. Thus, packet loss was ruled out.

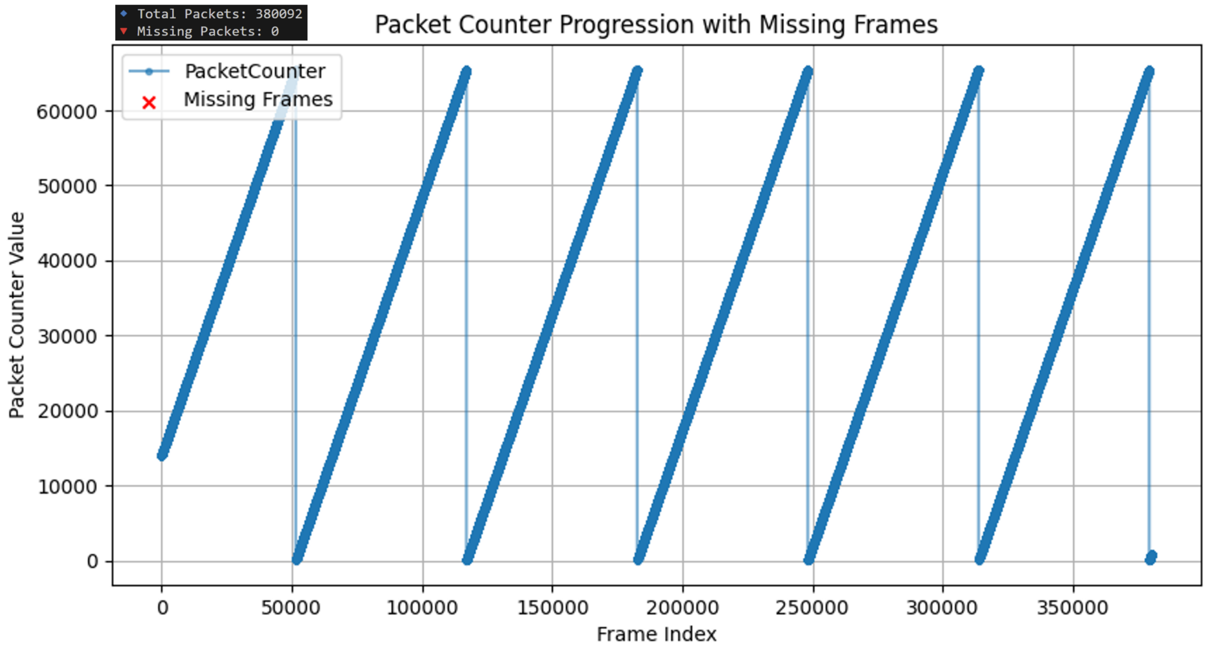

Figure 7.2: Packet counter progression across the full motion capture recording session. Each reset in the counter corresponds to the natural overflow of the 16-bit packet counter used by the Movella sensors. The blue line shows the continuous increment of the packet counter, and the red markers (none visible here) would indicate missing frames. As shown in the top-left overlay, a total of 380,092 packets were recorded with **zero missing frames**, confirming that packet loss was not responsible for observed timing inconsistencies. *Credit: By Author*

Stage II – Testing for Delay in Sending Triggers

Next, we considered whether there might be a delay in sending event triggers from the experiment code. To test this, we implemented internal logging in the PsychoPy script, recording each trigger event with two types of timestamps: PsychoPy's internal clock, which provides the time since the start of the experiment, and the system's Unix time, offering an absolute wall-clock reference.

By comparing the timestamps between consecutive events in the log file, we confirmed that the actual sending time matched exactly the intended experimental timing. For example, reaching trials were expected to occur every 5 seconds within trial blocks, and indeed we recorded events at consistent 5-second intervals, as programmed. This ruled out any issues in the timing of trigger transmission from the stimulus presentation software.

Event	PsychoPy Time	Unix Time
Experiment Start	14.016	1.74E+09
Sending marker 207	14.017	1.74E+09
Starting Run 1	16.23	1.74E+09
Sending marker 101	16.232	1.74E+09
Sending marker 200	16.434	1.74E+09
Sending marker 201	24.635	1.74E+09
Trial Block 1 Start (Run 1)	29.85	1.74E+09
Sending marker 202	29.852	1.74E+09
Starting Trial 1 in Block 1	30.555	1.74E+09
Displaying Target/Trajectory	30.557	1.74E+09
Sending marker 203	30.57	1.74E+09
Playing Beep Sound	30.772	1.74E+09
Sending marker 204	33.278	1.74E+09
Playing End Sound	33.48	1.74E+09
Starting Trial 2 in Block 1	36.044	1.74E+09
Displaying Target/Trajectory	36.046	1.74E+09
Sending marker 203	36.055	1.74E+09
Playing Beep Sound	36.256	1.74E+09
Sending marker 204	38.774	1.74E+09
Playing End Sound	38.976	1.74E+09
Starting Trial 3 in Block 1	41.53	1.74E+09
Displaying Target/Trajectory	41.532	1.74E+09
Sending marker 203	41.546	1.74E+09
Playing Beep Sound	41.748	1.74E+09
Sending marker 204	44.278	1.74E+09
Playing End Sound	44.48	1.74E+09

Figure 7.3: Log file output from PsychoPy showing the precise timing of experimental events. Each event is timestamped using both PsychoPy's internal clock and the Unix wall-clock time. *Credit: By Author*

Stage III - Testing for Delay in EEG Reception

We then explored the possibility that the EEG system might be receiving triggers with a delay. Since Biosemi records at a known fixed rate of 1024 Hz, we examined whether the time intervals between events, once converted from samples to seconds, were consistent with the programmed timing of events. As such, EEG events were extracted from the Biosemi BDF files using MNE-Python. Then, a script analyzed the time differences between each bracket of corresponding events (i.e. blocks) using the corresponding formula.

$$\text{Time Difference (s)} = \frac{\text{Sample Difference}}{1024}$$

The result confirmed that EEG event were received at consistent intervals aligned with the experiment structure. This ruled out any issues in the timing of trigger reception into the EEG system.

Stage IV - Estimating the Actual Sampling Rate of Motion Data

After confirming there were no issues With the EEG system, our attention returned to the MoCap system. We suspected that the sampling rate might not be the expected 120 Hz, possibly due to the use of MT Manager instead of MVN Pro. To test this, we computed the expected number of motion samples using the total duration of the EEG recording and compared it to the actual number of motion samples:

$$\text{Expected Samples} = \text{EEG Duration (s)} \times 120$$

We then compared this to:

$$\text{Actual Sampling Rate} = \frac{\text{Total Motion Samples}}{\text{EEG Duration (s)}}$$

This series of calculation revealed that the motion data was sampled at approximately 100.29 Hz, significantly lower than the 120 Hz sampling rate advertised. All calculations were mediated by custom Python scripts as illustrated by the output in Figure 7.4.

```
BDF file detected
Setting channel info structure...
Creating raw.info structure...
EEG Recording Duration: 3790.00 sec (3880960 samples)
Expected Motion Frames: 454800.00
Actual Motion Frames: 380092
Estimated Motion Sampling Rate: 100.29 Hz
⚠️Warning: Sampling rate mismatch detected!
```

Figure 7.4: Mismatch between expected and observed motion data sampling rate. The total number of motion samples falls short of the expected count based on EEG duration and advertised 120 Hz rate, suggesting a lower effective rate. *Credit: By Author*

Stage V - Verifying Sampling Rate Consistency

To determine if this rate was stable, we used event pairs (e.g., TARGET to RETURN) to segment motion data into discrete trials. For each segment, we computed the duration and number of motion samples. Trials showed a consistent sample count of around 100 samples for a 10-second segment, indicating a true sampling rate of approximately 100 Hz. This was also tested for all event pairs in our experiment, and findings were consistent as illustrated in Figure 7.5.

The small deviation (0.29 Hz) observed in Figure 7.4 is explained by an extra 10 seconds of motion data recorded after EEG stopped. This extra time is accounted for, since stopping the recording of data is done manually at the end of the experiment. We do this because some of the Biosemi discussion pages online have expressed that using the auto-save function via trigger bursts, can sometimes result in corrupted files.

```
Trial 13: Duration = 10.210s, Packets = 1021, Estimated Sampling Rate = 100.00 Hz
Trial 14: Duration = 10.200s, Packets = 1020, Estimated Sampling Rate = 100.00 Hz
Trial 15: Duration = 10.210s, Packets = 1021, Estimated Sampling Rate = 100.00 Hz
Trial 16: Duration = 10.210s, Packets = 1021, Estimated Sampling Rate = 100.00 Hz
Trial 17: Duration = 10.210s, Packets = 1021, Estimated Sampling Rate = 100.00 Hz
Trial 18: Duration = 10.210s, Packets = 1021, Estimated Sampling Rate = 100.00 Hz
Trial 19: Duration = 10.200s, Packets = 1020, Estimated Sampling Rate = 100.00 Hz
Trial 20: Duration = 10.200s, Packets = 1020, Estimated Sampling Rate = 100.00 Hz
Trial 21: Duration = 10.210s, Packets = 1021, Estimated Sampling Rate = 100.00 Hz
Trial 22: Duration = 10.200s, Packets = 1020, Estimated Sampling Rate = 100.00 Hz
Trial 23: Duration = 10.200s, Packets = 1020, Estimated Sampling Rate = 100.00 Hz
Trial 24: Duration = 10.210s, Packets = 1021, Estimated Sampling Rate = 100.00 Hz
Trial 25: Duration = 10.210s, Packets = 1021, Estimated Sampling Rate = 100.00 Hz
Trial 26: Duration = 10.200s, Packets = 1020, Estimated Sampling Rate = 100.00 Hz
Trial 27: Duration = 10.200s, Packets = 1020, Estimated Sampling Rate = 100.00 Hz
Trial 28: Duration = 10.200s, Packets = 1020, Estimated Sampling Rate = 100.00 Hz
Trial 29: Duration = 10.200s, Packets = 1020, Estimated Sampling Rate = 100.00 Hz
Trial 30: Duration = 10.210s, Packets = 1021, Estimated Sampling Rate = 100.00 Hz
Trial 31: Duration = 10.220s, Packets = 1022, Estimated Sampling Rate = 100.00 Hz
Trial 32: Duration = 10.210s, Packets = 1021, Estimated Sampling Rate = 100.00 Hz

Estimated True Motion Sampling Rate for 205 -> 200: 100.00 Hz
```

Figure 7.5: Trial-by-trial sampling rate analysis confirms consistency around 100 Hz. *Credit: By Author*

Stage VI - Initial Trigger Interpretation Correction

Upon further investigation, we discovered that using the MNE function **`mne.find_events(raw, stim_channel='Status', initial_event=True)`** introduced an earlier event at the very start of the EEG stream. By default **`initial_event`** is set to **`False`**, which discards this first event. However, enabling this flag revealed an additional trigger occurring approximately 0.82 seconds earlier than the initially assumed synchronization marker.

This first trigger corresponds to the TTL pulse emitted from the Awinda Station as soon as recording begins. The exact nature of the second trigger has not been identified. However, when accounting for this shift, we recovered the consistent alignment that we expected in the first place. In order to get proper alignment, we had to consider the initial event at the start, and then shift all the triggers back by this 0.82 seconds offset. In fact, it was better to set this as a variable, and correct it dynamically, as the actual offset would hover around that value from one recording session to the next.

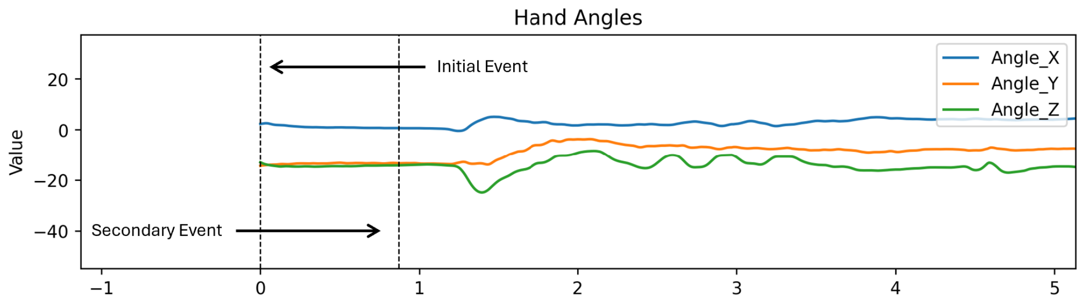

Figure 7.6: Initial and Secondary synchronization trigger events at the start of data recording. *Credit: By Author*

Stage VII - Final Timing Verification

Events on the raw motion file showed that movement onset now aligned as expected: roughly 300–450 ms after the synchronization trigger (see Figure 7.7). Given that the experiment intentionally delays stimulus onset by 200 ms (to avoid jitter), this leaves a participant reaction time of about 250 ms, matching previously published values in motor imagery experiments such as [Pancholi et al., 2022]. We verify by computing average reaction times over all trials and find a value of around 246 ms. The reaction times range from 200 to 300 ms.

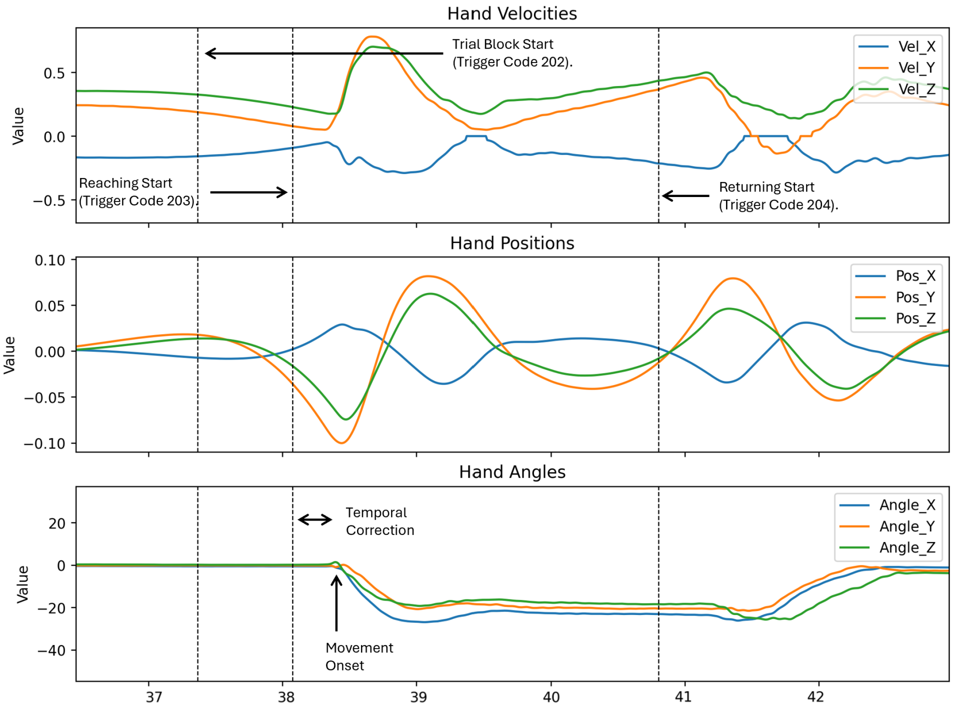

Figure 7.7: Example of motion data from a single trial illustrating a corrected trigger alignment. The delay between the actual onset of movement and trigger event has been corrected, illustrating correct temporal order in execution of movement, which should occur shortly after the cue.

We also observe that movement onset begins at the exact time as recorded by the tracker on MT Manager (see Figure 7.8) before exporting the data. This increases confidence in the synchronization and alignment startegies.

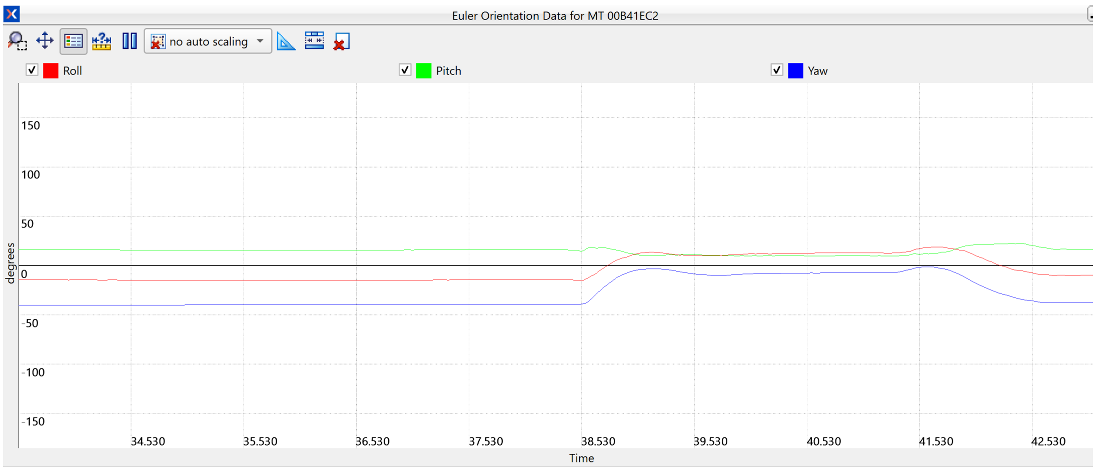

Figure 7.8: Trial-by-trial sampling rate analysis confirms consistency around 100 Hz, validating the true sampling rate of the motion capture system despite initial assumptions. *Credit: By Author*

In conclusion, we show in this section our validation process of the alignment between the EEG and MoCap data streams. By working through a series of possible causes for the initial timing mismatch, we were able to identify and correct the problem. Once adjustments were made, namely accounting for the true motion sampling rate and the shift of the initial synchronization trigger, the data showed clear and consistent alignment across all trials. These results confirm that our synchronization method worked as intended and that our recordings are well-suited for further analysis.

7.1.2 Data Pipeline – From Raw Signals to Labeled Dataset

Data Pipeline Workflow

The final dataset was stored in HDF5 format and organized hierarchically by participant, run, and trial (see Figure 7.9). Each trial segment includes synchronized EEG and MoCap data stored in a modular structure. Segments are further divided into experimental phases such as reaching and returning allowing for targeted analysis of specific periods within each trial (see Figure 7.10).

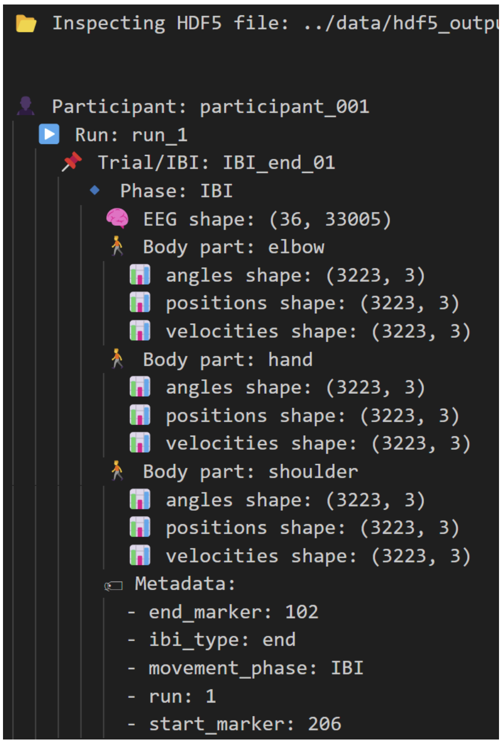

Figure 7.9: Overview of the dataset structure, including EEG and motion data for the IBI block, and the accompanying metadata used for indexing and analysis. *Credit: By Author*

For each phase, EEG data is stored as a multi-channel array, while MoCap data is available for key upper limb joints including the hand, elbow, and shoulder as illustrated in Figure 7.10. Motion features include estimated joint angles, positions, and velocities in three-dimensional space. This structure ensures that all relevant sensor modalities are accessible and aligned within a common temporal frame.

Accompanying each data segment is a range of metadata attributes. These include the condition type (executed vs. imagined), target id, block number, repetition number, and goal type (target or trajectory). This metadata enables flexible querying, filtering, and segmentation of the dataset for various downstream analysis and modeling tasks.

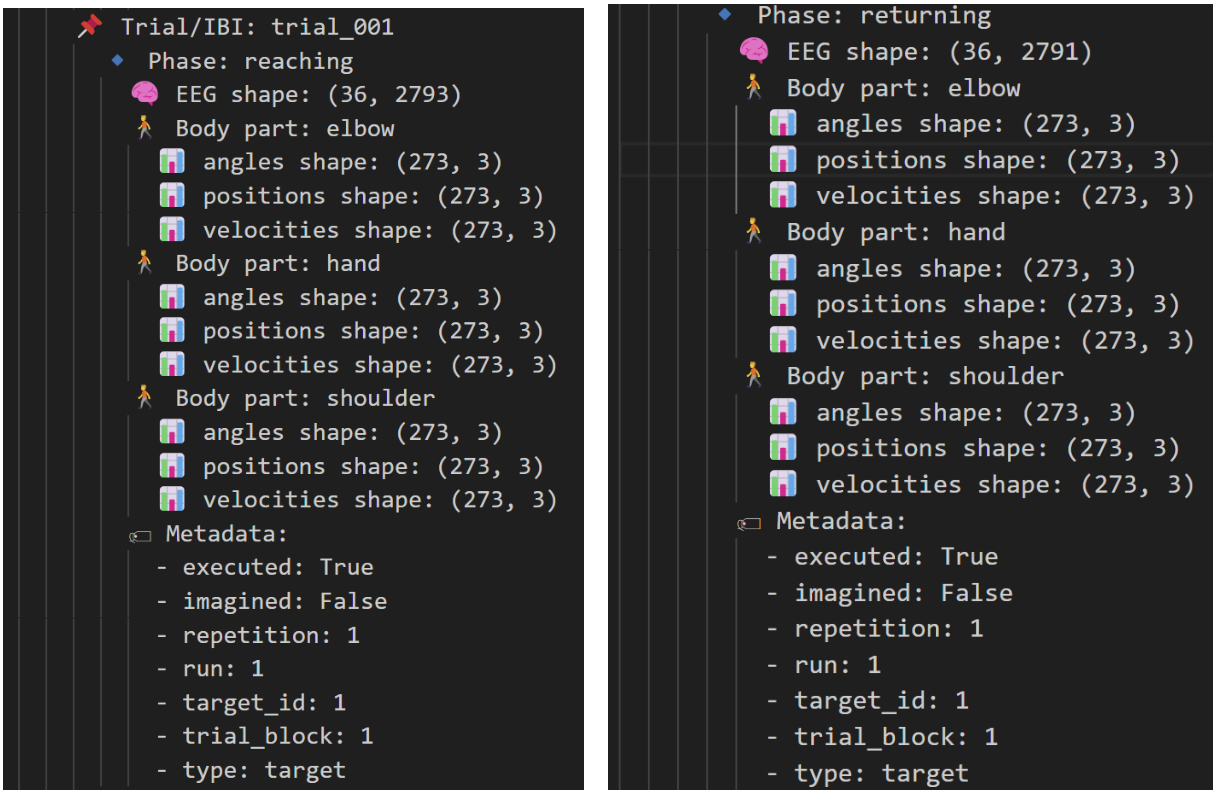

Figure 7.10: Overview of the dataset structure, showcasing the first trial. Notice that the trial is split into a reaching and returning phase respectively with corresponding metadata allowing for fine-grained analysis of various stages of movement. *Credit: By Author*

EEG & Motion Data Pre-processing

Following the preprocessing steps described in Section 7.1.2, we inspected the cleaned EEG and motion signals to evaluate the effectiveness of artifact removal strategies and the overall data quality for downstream tasks.

EEG Data

In order to demonstrate the impact of these preprocessing steps, we analyzed a representative EEG trial in which event-related potentials were visible on channels PO3, O1, Oz, O2 and, PO4 following a visual cue. The raw signal, as shown in Figure 7.11a, is heavily contaminated by line noise and low-frequency drifts. After applying notch and bandpass filters, followed by Independent Component Analysis (ICA), the resulting signal shows clear suppression of contaminating artifacts and highlights the event-related potentials (see Figure 7.11c).

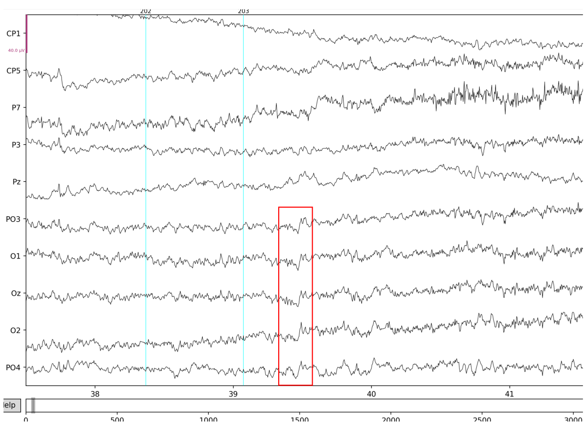

(a) Before preprocessing. High-frequency noise and drifts dominate.

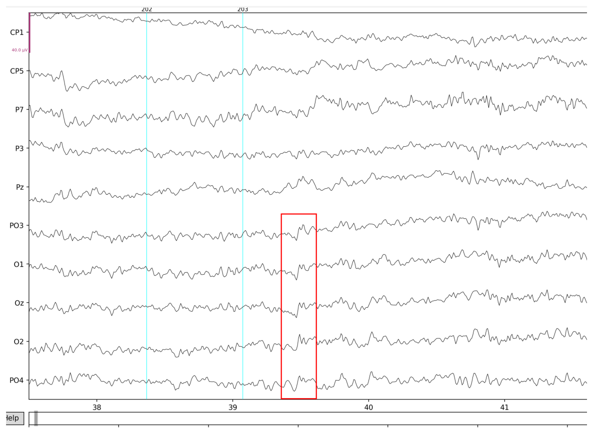

(b) After notch and bandpass filtering. Event-related potentials become more visible.

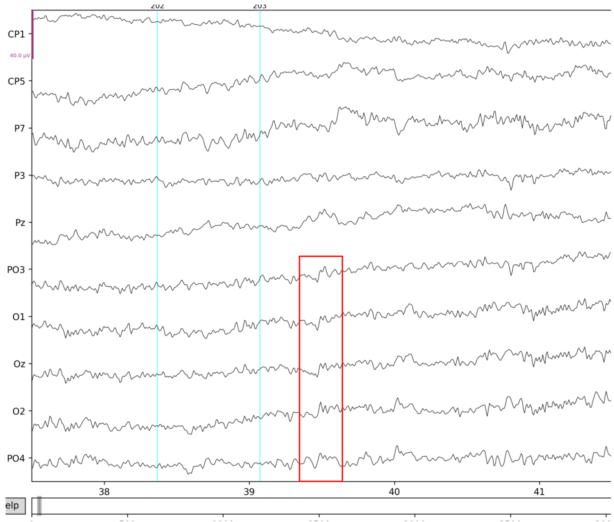

(c) After ICA artifact removal. Eye and muscle artifacts are suppressed, improving clarity.

Figure 7.11: Effect of EEG preprocessing on evoked potentials for a representative trial. *Credit: By Author*

Figure 7.12a shows an example trial that was affected by motion and ocular artifacts. In the raw EEG, large fluctuations obscure the underlying neural activity (see Figure 7.12a). After applying notch and bandpass filters, followed by ICA, the signal quality improves (see Figure 7.12b). The EOG signal recorded during the trial confirms the presence of eye movements (see Figure 7.12c), which were used to identify and remove associated components through ICA.

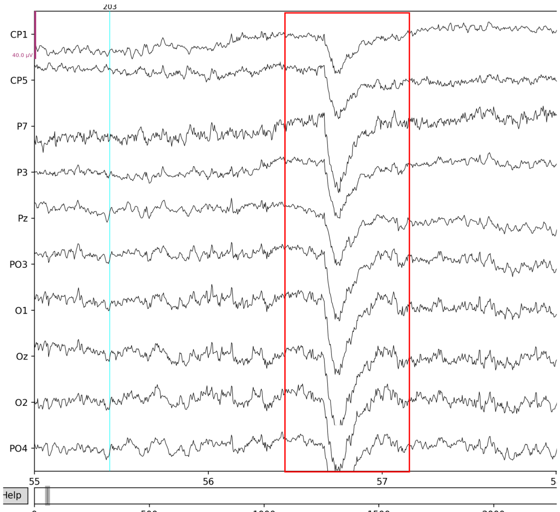

(a) Raw EEG segment from an executed trial showing motion and eye related artifacts.

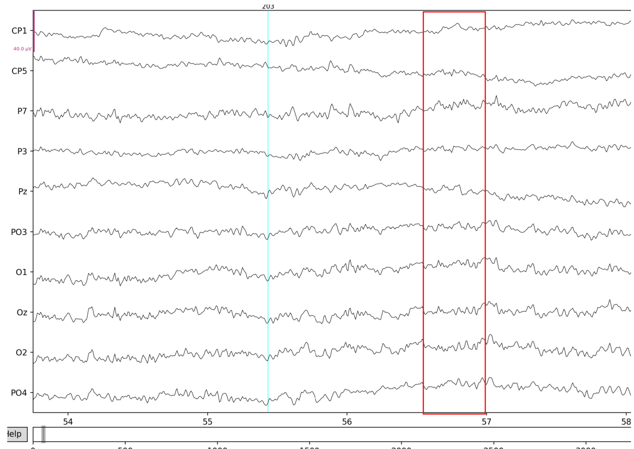

(b) Same trial after filtering and ICA. Artifacts are substantially reduced, and task-related activity becomes more visible.

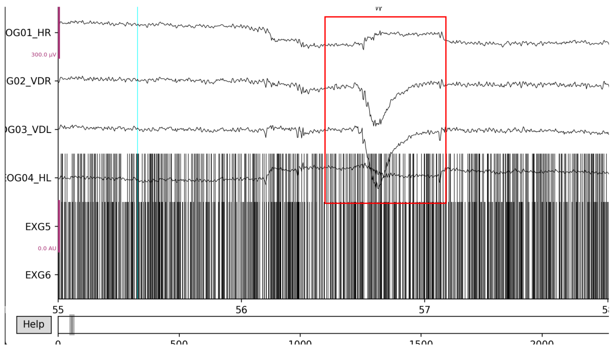

(c) EOG recording from the same trial, highlighting eye movement activity used to guide ICA artifact removal.

Figure 7.12: Illustrative example of EEG artifact removal through filtering and ICA with EOG signals. *Credit: By Author*

Additionally, we present a baseline (rest) segment before and after preprocessing (see Figure 7.13a, Figure 7.13b). In this case, two distinct artifacts were present. One was successfully removed through ICA, while the other persisted. Due to the sensitive trade-off between removing noise and preserving brain signals, ICA was set to 26 components. Using a larger value risked removing meaningful signals.

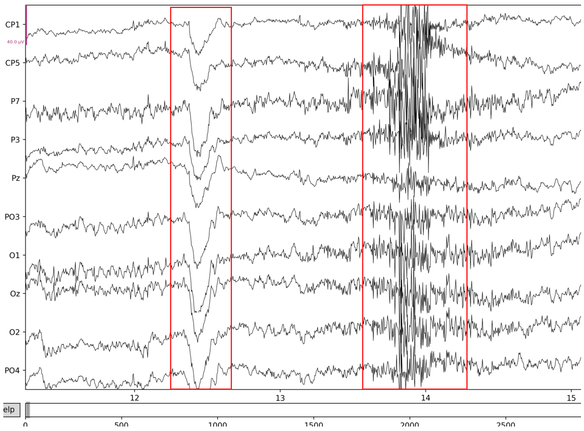

(a) Raw EEG during a baseline segment, showing two noticeable artifacts.

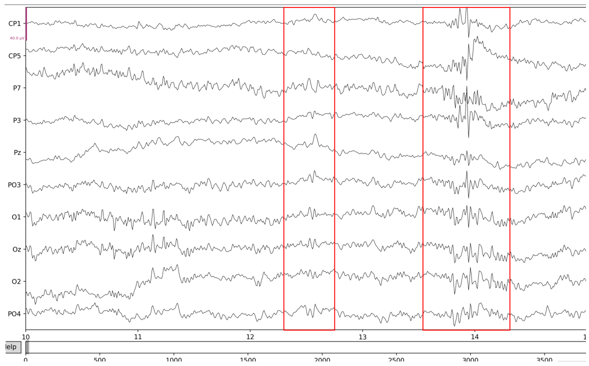

(b) Same baseline segment after filtering and ICA. One artifact is successfully removed, while the other remains.

Figure 7.13: Partial artifact removal in baseline EEG using filtering and ICA. *Credit: By Author*

These examples demonstrate that preprocessing greatly improves EEG signal quality and helps reveal neural responses. However, some residual artifacts such as facial or neck muscle movements may remain. This is a common limitation in EEG recordings involving movement and should be considered when analyzing the data.

Kinematic Data

Preprocessing motion data was significantly more challenging, mainly because of the cumulative effects of integration drift in estimating velocity and position. Several cleaning techniques were implemented and evaluated as outlined in Section 6.1.7.

Using a high-pass and low-pass filter was crucial, as otherwise the integration of accelerometer data resulted in unrealistic growth in velocity and position over time, often diverging toward infinity as illustrated in Figure 7.14.

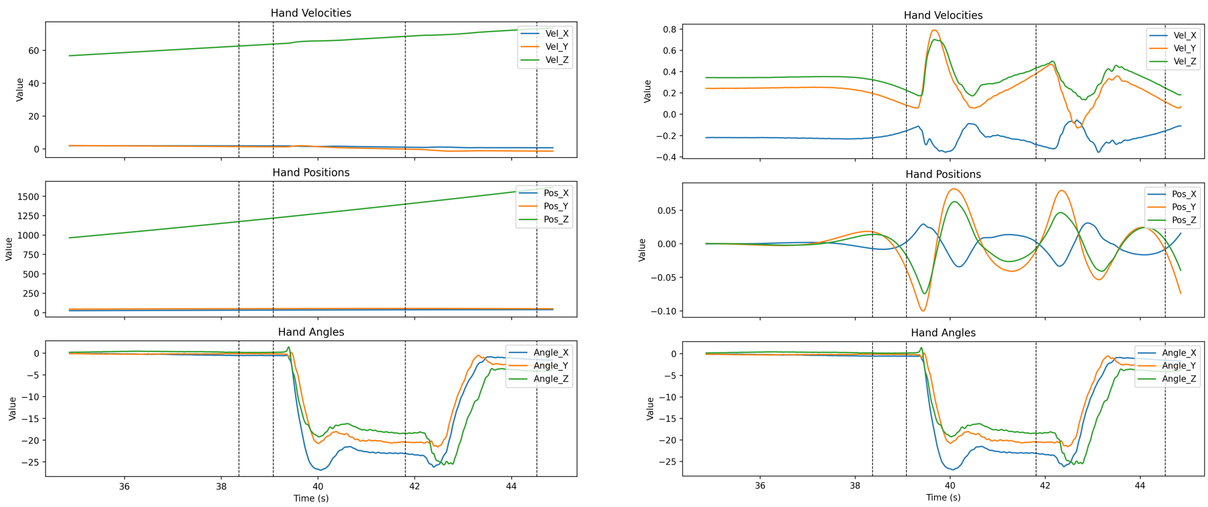

Figure 7.14: Effect of high-pass and low-pass filtering on position and velocity signals. Without filtering (left), drift accumulates rapidly. *Credit: By Author*

Despite the use of several preprocessing methods (Kalman smoothing and baseline correction) no perceivable improvements were observed in velocity or position signals. Zero Velocity Update (ZUPT) was the only method to show a measurable effect. When applied with a high threshold, it aggressively zeroed out movement, suppressing true motion signals; at lower thresholds, it missed stationary periods entirely. Figure 7.15 compares the impact of different ZUPT thresholds. Any value lower than the ones shown would result in no change in the data, making it identical to Figure 7.14 (b).

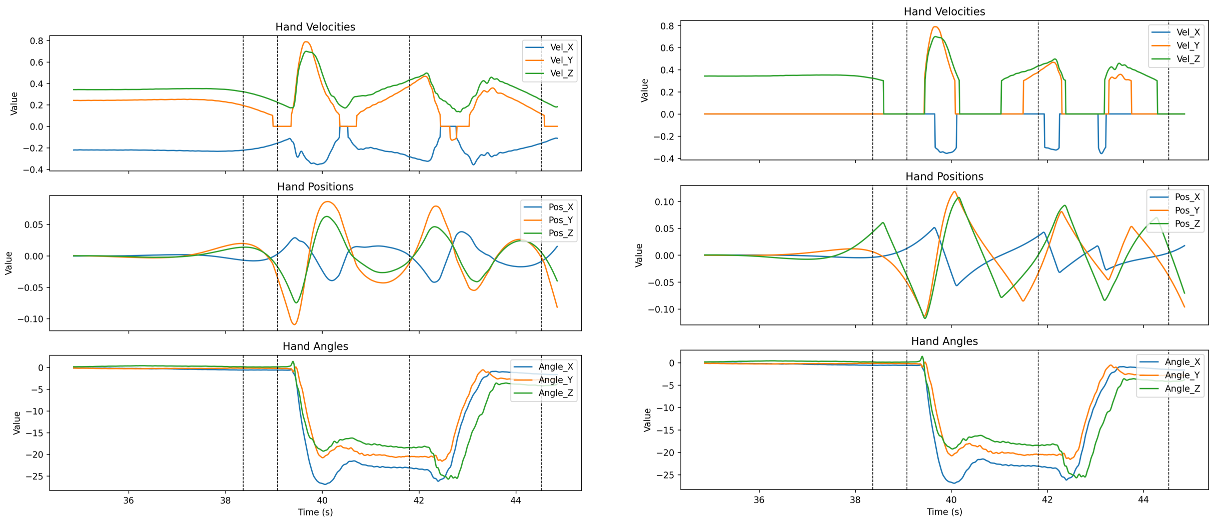

Figure 7.15: Comparison of ZUPT performance with low (0.1) vs. high thresholds (0.3). *Credit: By Author*

In all trials, movement seemed to start before the visual cue appeared, which should not happen. This was caused by small errors in the acceleration data adding up during the integration process used to compute velocity and position. As a result, these derived features became unreliable and were excluded from the analysis.

On the other hand, angular orientation data remained mostly stable and accurate throughout the recordings. This is because it was taken directly from the sensor's gyroscope readings, rather than being calculated from acceleration data. This could have been used to make a more elaborate version of ZUPT. However, this was beyond the scope of this work.

Electromagnetic Interference

During one recording session, we observed a change in the EEG signal that coincided with an incoming phone notification in the room. While this kind of interference didn't happen often, it showed us how important it was to keep the recording environment free of electrical noise. To avoid similar issues, we had to be strict about lab conditions. In subsequent recording sessions, we would request from participants to leave all electronic items in a separate room with lockers before starting the experiment.

We also started considering the possibility of further contamination from the various electronic devices which are native to the lab room, such as the desktops, laptops, and crucially the Awinda station itself, which wirelessly communicates with the trackers. To investigate this, one could perform an ablation analysis by systematically turning off each electronic device and comparing the resulting EEG signal quality across conditions, helping to isolate and identify specific sources of Electromagnetic Interference (EMF). Later on, these frequencies can be specifically targeted in preprocessing steps.

7.1.3 Limitations Encountered and Pivot to Public Dataset

Although a significant portion of this project was dedicated to the design, implementation, and refinement of a custom multimodal experiment and data collection pipeline, the resulting self-collected dataset ultimately proved unusable for modeling. The limitations encountered can be grouped into three main categories: technical challenges, participant-related constraints, and paradigm inconsistencies.

Technical Challenges with Data Quality

While the EEG data quality improved after preprocessing, some residual noise remained in the recordings. These artifacts, including muscle movements and low-frequency drift, were partially but not fully suppressed. Nonetheless, the EEG signal was generally usable on the condition of accounting for EMF in subsequent recording sessions. In contrast, the MoCap data presented more severe limitations. Despite the application of several preprocessing methods, velocity and position data suffered from significant drift. Errors accumulated during integration, making these features unreliable across trials. Furthermore, the motion capture system operated at an effective sampling rate of 100 Hz (rather than the advertised 120 Hz), which introduced additional uncertainties. After all, only angular data remained usable.

Lack of Participant Availability

Another limitation was the inability to continue data collection. By the time the experimental protocol had been finalized and the synchronization and preprocessing pipelines were fully operational, the two participants who had initially supported the development process were no longer available. Despite significant efforts to recruit new participants via flyer distribution, lab networks, and in-person requests, no additional volunteers were secured. As a result, collecting a new, clean dataset from scratch within the project's time constraints was not feasible.

Variability in Motor Imagery Strategy

During the early recording sessions, participants engaged with the motor imagery task differently. Some imagined the movement visually, while others relied on a kinesthetic sensation. This difference, while expected, added uncontrolled differences in mental strategy that likely influenced the neural pathway used. This would mean that making comparisons between participants would be less interpretable.

Decision

As a result, the decision to exclude the self-collected dataset from downstream tasks was made. The preprocessing pipeline remains functional and well-documented, and several recommendations have been made in improving future versions. However, to move forward constructively within the thesis timeline, a change was made to use an existing public dataset of better signal quality and larger participant coverage, albeit with reduced customization (motor imagery not included). The details of this pivot and the new dataset are discussed in Part B of the thesis.

7.2 Part B: Theoretical Approach – Modeling Internal Motor Representations

This section presents the outcomes of the analyses described in Section 6.2.6. The results reflect both qualitative and quantitative insights gained through testing and adapting the MARBLE framework for structured EEG decoding. The first two replication tasks made use of MARBLE's public Github repository [1].

7.2.1 Replicating Latent Flow Fields with MARBLE

Here we provide the results of the first experiment. The latent structure that MARBLE extracted from the vector fields was visualized through four key plots: embeddings, flow fields, histograms of feature activations, and a neighborhood similarity graph.

(a) Latent space embedding of four vector field types. Clustering reflects correct grouping of dynamics by type. *Credit: By [Gosztolai et al., 2025]*

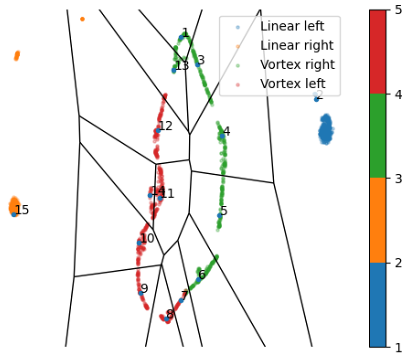

(b) MARBLE-inferred vector field reconstruction over the latent space, showing internal smooth flow directions across the manifold. *Credit: By [Gosztolai et al., 2025]*

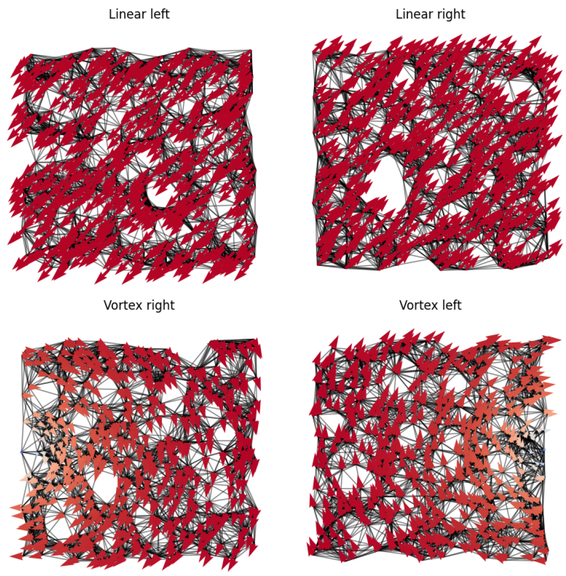

Figure 7.16: Visualization of MARBLE's latent manifold learning from synthetic vector field data. (a) The learned 2D embedding shows clustering of the four input dynamics, indicating successful separation. (b) The corresponding inferred flow fields in the latent space demonstrate smooth vector field reconstruction, revealing the model's ability to capture internal dynamics across the manifold. *Credit: By [Gosztolai et al., 2025]*

Figure 7.16a confirms that MARBLE successfully separated the four vector field types into distinct clusters. The flow field plot (see Figure 7.16b) further illustrates how these embeddings maintain internal temporal continuity, with smooth vector directions over the latent space.

The analysis was extended with feature-level visualizations. The histograms in Figure 7.17a shows how different neural features become active across different inputs, and Figure 7.17b

[1] https://github.com/Dynamics-of-Neural-Systems-Lab/MARBLE/tree/main

shows local motifs. The latter illustrates how MARBLE learns to capture spatially and temporally adjacent representations. Even with simple input patterns, the learned feature types were diverse and organized.

(a) Distribution of learned features across different vector fields. Distinct activation patterns emerged for each class. *Credit: By [Gosztolai et al., 2025]*

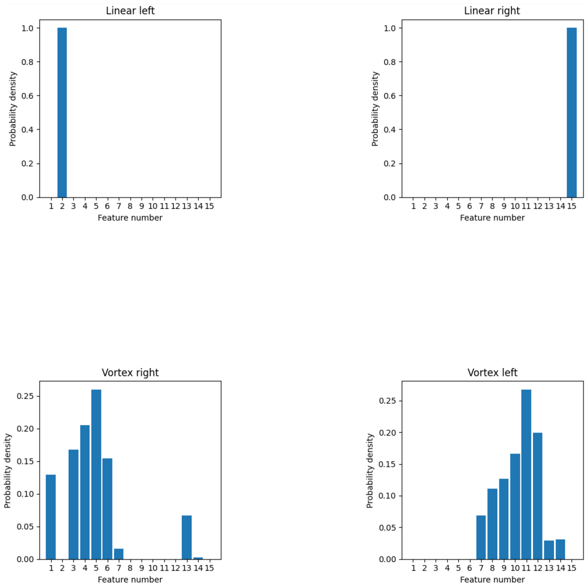

(b) Local motifs identified over the latent space. *Credit: By [Gosztolai et al., 2025]*

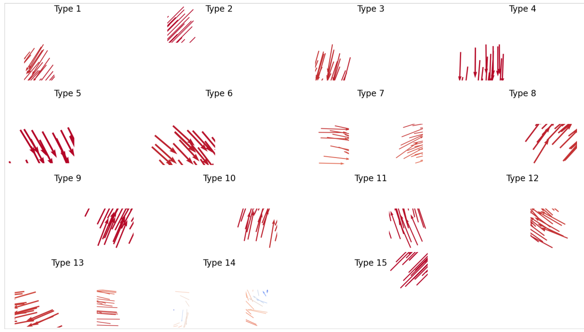

Overall, these results confirmed that MARBLE works as intended and helped us better understand how it shapes a low-dimensional latent structure that captures patterns both specially and temporally. Even with very simple input data, the model was able to separate different patterns clearly and organize them. This makes it a strong candidate for future use in decoding brain activity from EEG signals.

7.2.2 Replicating the Monkey Reaching Task with MARBLE

The MARBLE pipeline successfully generated low-dimensional latent embeddings that preserved the structure of the reaching task. When viewed using PCA and UMAP projections, these embeddings show clear clustering by target direction. This demonstrates the model's ability to separate neural trajectories based on the monkey's intended movement.

Figure 7.18 shows the MARBLE-generated latent embeddings. Each point represents a neural state at a given time, colored by the reach direction condition. The distinct clusters confirm that MARBLE encoded task-relevant differences in neural activity in an unsupervised setting. Locally, these embeddings are organized as flow fields (see Figure 7.16), which represent how neural activity evolves over time.

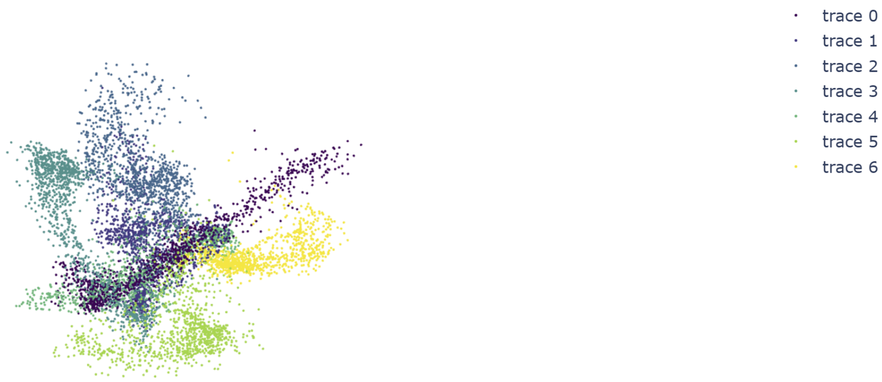

Figure 7.18: MARBLE-generated latent embeddings from macaque spiking activity. Each dot represents the neural state at a point in time, colored by reach direction. *Credit: By [Gosztolai et al., 2025]*

These embeddings were also evaluated in decoding hand kinematics. A regression model was trained to predict the reaching trajectories from the MARBLE embeddings. As shown in Figure 7.19, the decoded trajectories closely matched the true movements across all directions, confirming that the learned latent representations retained detailed motor information.

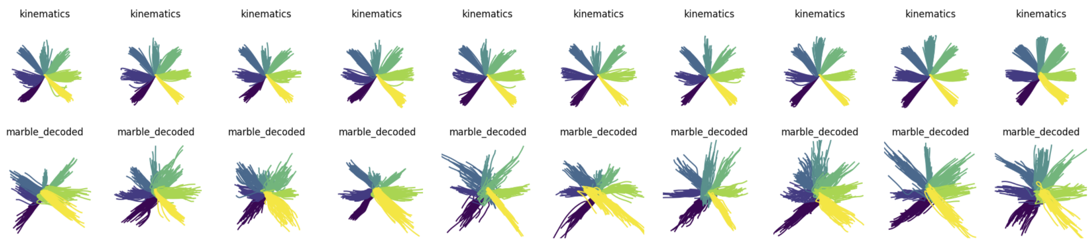

Figure 7.19: Ground-truth hand kinematics (top) and corresponding trajectories decoded from MARBLE embeddings (bottom). *Credit: By [Gosztolai et al., 2025]*

Together, these results demonstrate MARBLE's ability to uncover the internal dynamics of motor intention from intracranial recordings. The latent space both separates reach directions and preserves detailed kinematic information for accurate decoding. These findings further support the use of MARBLE for structured decoding of EEG.

7.2.3 WAY-EEG-GAL with MARBLE

Preparing WAY-EEG-GAL for MARBLE

The goal of this experiment was to reformat the WAY-EEG-GAL dataset into a structure compatible with MARBLE. We successfully developed and executed a modular preprocessing pipeline, which performed the following:

- Extracted raw EEG and kinematic data across sessions and participants.
- Loaded and aligned trial metadata using annotated event markers.
- Applied filtering, band decomposition, and standardization to EEG signals.

- Binned the EEG signals into 20 ms non-overlapping rate-like representations.
- Performed Principal Component Analysis (PCA) to reduce dimensionality while preserving neural variance.

To determine the appropriate number of principal components for MARBLE input, we applied PCA separately to each EEG frequency band: *alpha*, *beta*, *delta*, *gamma*, and the full-band (*total*). Figures 7.20 and 7.21 present the cumulative variance explained across increasing numbers of principal components for each frequency band. The number of components needed to reach 90% variance varied across bands, highlighting differences in signal complexity and potential decoding relevance.

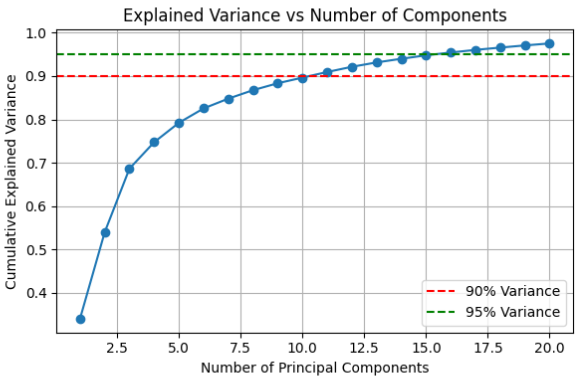

(a) Alpha band – 11 components

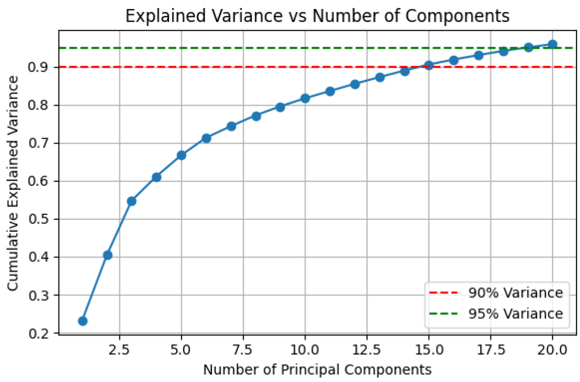

(b) Beta band – 15 components

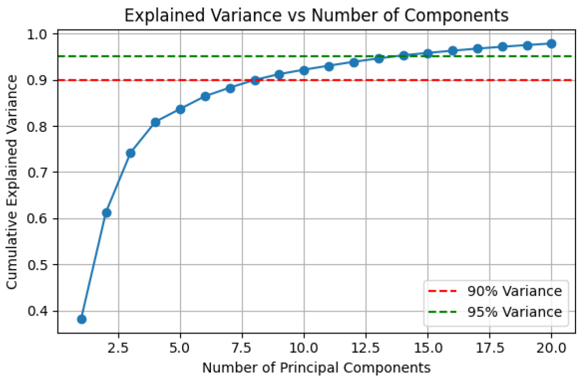

(c) Delta band – 9 components

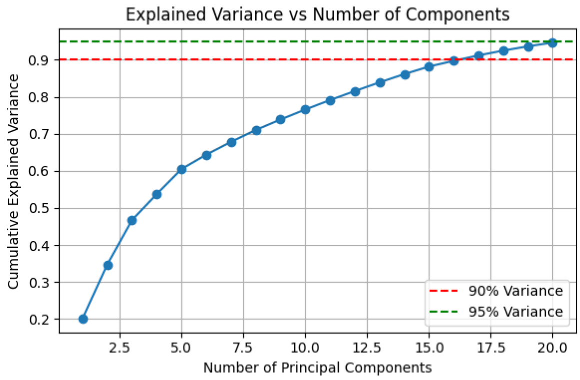

(d) Gamma band – 17 components

Figure 7.20: Cumulative variance explained per frequency band. Dashed lines indicate 90% (red) and 95% (green) thresholds. *Credit: By Author*

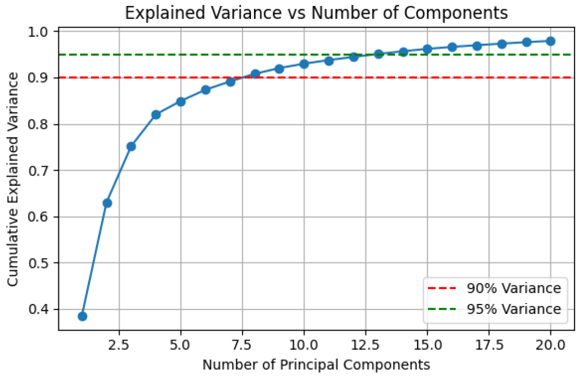

Figure 7.21: PCA variance explained for the **total band** (full-spectrum EEG). 8 components are required to explain 90% of the total variance. *Credit: By Author*

These PCA results reveal how information is spread across EEG channels in each frequency band. For instance, the *delta*, *alpha*, and *total* bands required fewer principal components. This suggests that the information they carry is more globally organized or redundant across channels. In contrast, the *beta* and especially *gamma* bands required many more components to reach the same variance threshold, indicating more spatially complex or localized activity. Prior studies have shown that each frequency band carries distinct information about brain function, particularly during movement planning and execution. For example, Ottenhoff et al. [2025] observed that each band reflects a different layer of brain organization, from large-scale coordination (*delta*) to detailed local computation (*gamma*).

This analysis is crucial for future steps, since it shows that fine-tuning the dimensionality of MARBLE's input to each frequency band may help the model better capture their unique contribution to motor representation, in turn shedding light on the role that these various frequencies play in movement.

The processed dataset now contains PCA-reduced neural data organized by trial and movement condition.

Running MARBLE with WAY-EEG-GAL dataset

Here we report the results of early experiments with the goal of assessing the validity of the MARBLE framework with EEG data. The initial MARBLE runs on the WAY-EEG-GAL dataset yielded consistently high validation losses across all tested configurations (see Figure 7.22).

While some low-dimensional embeddings displayed early signs of clustering as shown in Figure 7.23, but these were inconsistent across runs and sensitive to hyperparameter settings. These embeddings could not be considered reliable due to poor convergence.

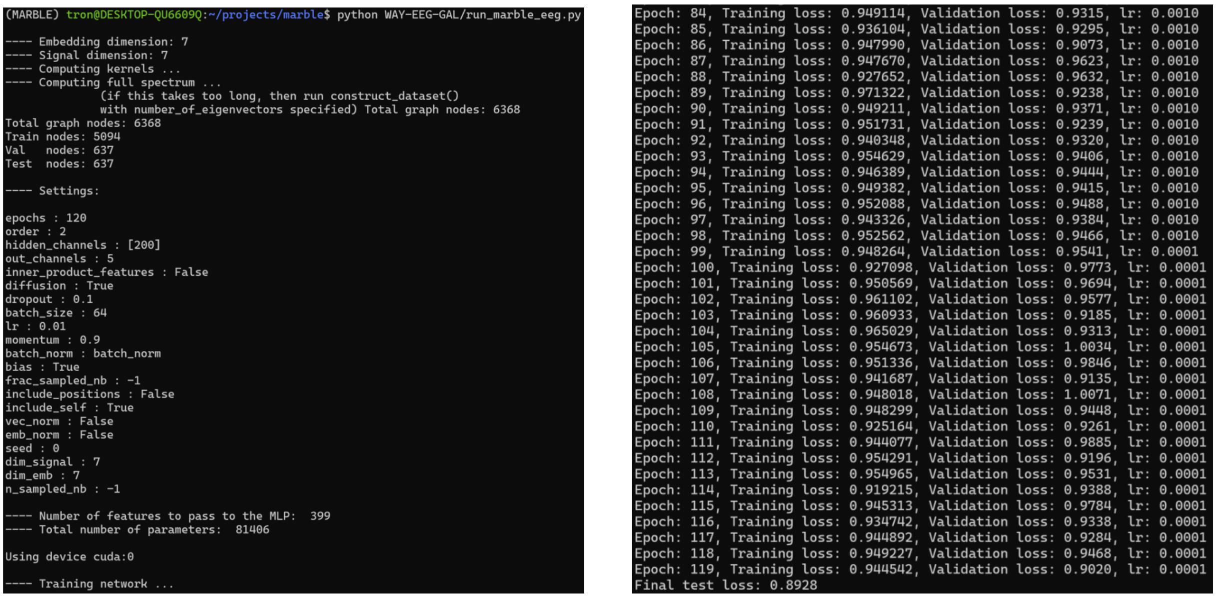

Figure 7.22: Attempted MARBLE configuration with corresponding validation loss. *Credit: MARBLE GitHub (Dynamics of Neural Systems Lab, 2023), Adapted by Author*

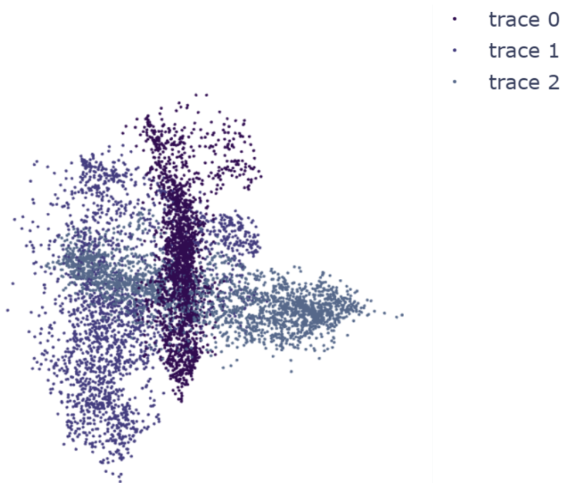

Figure 7.23: Example of MARBLE-generated latent embeddings from EEG data using the WAY-EEG-GAL dataset. *Credit: MARBLE GitHub (Dynamics of Neural Systems Lab, 2023), Adapted by Author*

Readers might be inclined to conclude that the results are not interpretable. However, the initiated eye will recognize the value in these observations. To make it clearer, it is best to contextualize these outcomes:

Cautious Interpretation:
Results reflect early-stage, minimally tuned experimentation. Furthermore, high validation loss does not imply that EEG is incompatible with manifold learning. Rather, these results imply that MARBLE may require architectural or preprocessing adaptations tailored to EEG.

Theoretical Support for Compatibility:
Several examples in the literature have provided direct evidence for such applications of manifold learning using EEG data. Thought Chart shows EEG connectivity forming latent manifolds

of mental states [Xing et al., 2016]. Riemannian classifiers provide interpretable EEG embeddings using covariance and wavelets [Paillard et al., 2024]. Finally, EEG microstates suggest underlying low-dimensional structures [Michel and Koenig, 2018], showcasing the presence of essential neural patterns for MARBLE learning.

Challenges with EEG:
We also identified several challenges specific to EEG-MARBLE integration, such as volume conduction, low spatial resolution, and the need for preprocessing to reveal neural geometry. These challenges relate mainly to the issue of source localization, such that it becomes intractable for the model to recognize spatial contribution of different channel locations, which not only reflect the activity of several populations of neurons, but alos overlap with readings from neighboring channels. These challenges are met with proposed enhancements, including wavelet-based features, covariance modeling, and architectural modifications such as Riemannian layers or graph-based encodings.

7.2.4 Part B: Summary of Results

The analyses in Part B explored the feasibility and benefits of using MARBLE for EEG decoding. The first experiment, using toy vector fields, demonstrated that MARBLE successfully learns smooth, temporally coherent latent spaces from synthetic inputs. This provides an understanding into the model's internal mechanics and the concept of flow fields.

The second experiment replicated MARBLE's application to intracranial monkey recordings, confirming that its latent embeddings preserve both class-level separation and fine-grained motor trajectories suitable for decoding.

The final experiment focused on adapting the WAY-EEG-GAL dataset as a temporary placeholder in the absence of our dataset. A modular pipeline was built to segment, filter, decompose, and reduce the EEG signal through PCA, yielding representations ready for downstream input. PCA results showed that slower bands like *delta* and *alpha* required less components than faster bands like *gamma* and *beta*. We also make early attempts at training the MARBLE framework with EEG data, however we do not get any concluding results. Rather, thorough analysis suggests some fine-tuning that would allow for processing our non-invasive neural data with MARBLE.

Together, these results support the theoretical shift toward structure-aware latent modeling in EEG decoding and lay a strong foundation for future work. However, due to time constraints and technical adaptation challenges, we were unable to complete the final MARBLE validation phase using the EEG dataset.

Chapter 8

Discussion

The pipeline in Part A highlighted significant challenges in simultaneous EEG-MoCap studies. While EEG preprocessing revealed meaningful evoked potentials, MoCap velocities and positions suffered from cumulative drift and an unexpected sampling rate, despite hardware specifications. Participant recruitment constraints and variability in their experimental strategies further limited the dataset. These findings emphasize the practical difficulty in obtaining large, high-quality multimodal recordings for continuous decoding.

These setbacks along with supporting literature pushed us to adapt our methodology toward latent modeling in Part B. By employing MARBLE's contrastive embedding of neural sequences into smooth latent flow fields, we leverage the brain's use of structured representations rather than treating EEG as unstructured input. Experiments on synthetic vector fields and macaque datasets confirmed the model's ability to separate movement classes and preserve detailed kinematic details in an unsupervised manner.

Experiments on the WAY-EEG-GAL dataset demonstrated the preprocessing requirements and formatting specifications for correct adaptation of EEG data to the MARBLE approach. We had hoped to demonstrate decoding of kinematic parameters from EEG using this approach. The expected outcome would have been distinct neural trajectories representing different movement conditions. Furthermore, it would have been relevant to investigate cross-subject decoding performance can be enhanced by leveraging this approach of modeling neural dynamics, which allows for potentially uncovering similar computational structures that could be reused across participants. Crucially, the model might have been capable of locating the overlapping patterns between executed and imagined movements, thus increasing decoding accuracy of imagined trajectories. Finally, compositionality and generalizing to unseen movements could be verified.

The intended direction after the setback in Part A, involved validating our theoretical approach of using manifold learning on the public dataset, which allows for a wide array of test to be conducted and for comparison with other work using this dataset. Crucially however, the intention was to later replace this by data collected using our own experiment and pipeline. That is because our own implementation benefited from a level of customization and diverse movement types that is absent from most public dataset.

Although the thesis might seem disconnected due to the A and B narratives. However, it is important to note that this dual narrative actually converges onto the same final goal, by complementing each other. Part A provides access to data in a format which is absent from public dataset, allowing for crucial research questions to be investigated by employing the developments in Part B, which crucially informed us about movement representation and modeling strategies.

Chapter 9

Conclusion

This thesis contributes a dual foundation for EEG-based continuous motor decoding. First, it details the design, synchronization, and preprocessing pipelines necessary for simultaneous EEG and MoCap recording, and documents the technical and logistical limitations encountered. Second, it establishes a theoretical shift toward latent manifold models which better align with the brain's structured, compositional representation of movement. While practical application to the collected dataset remains future work, the demonstrated success on synthetic and public invasive neural datasets lays the foundation for generalizable continuous decoding of both executed and imagined movements. Future efforts will collect new multimodal data under the established refined protocols and apply MARBLE end-to-end, aiming to realize naturalistic, continuous BCI control.

Appendix A

Consent Form

For the research

Decoding 3D Upper Limb Motion Using EEG and Motion Capture Integration: A Deep Learning Approach

it is necessary to use personal data. To use this data during our research we need your consent.

Goal of the research.

The goal of the research is to identify brain activity which maps to the movement of your upper limbs. Hence, we aim to develop a decoder based on AI which is able to reconstruct the trajectory of your upper limbs (right wrist, elbow, and shoulder).

How does the study work?

You will have to perform a task that involves moving your hand from a rest position (on the chair handles) to one of five target positions. Then you will return your hand to the rest position. This will be repeated several times, and your movements towards the target and back will be queued by a sound. You will subsequently be asked to perform the same experiment, however this time you will be asked to imagine moving your hand towards that target.

The activity in the brain is recorded by placing a cap with electrodes on your head. The cap ties under the chin. To get good contact between the electrode and the head, electrode gel is used (this makes your hair sticky).

The kinematic data will be recorded using a motion capture suit which you will be asked to wear.

Time.

A full session lasts about 60 minutes.

What are the risks?

There are no risks involved in participating in this study.

Data collected.

The following data is being used:

- *First name and last name: this is used solely to address you in our communications*.
- *E-mail address: this is used for communication*.
- *Gender: this is used since EEG brain activity is different between genders*.
- *Age: this is used for auditing age groups within the study*.
- *EEG (electroencephalogram): brain activity data which will be used along with the motion data to train the AI regression model*.
- *Kinematic Data: the motion of your upper limbs (right wrist, elbow, and shoulder) which will be used along with the EEG data to train the AI regression model*.

Data storage and use.

Data that can be traced back to you will also be *anonymized. Additionally, your personal data (as listed previously) will not be stored with your brain activity or motion data. Instead, we will use a conversion list to recognize the data belongs to whom. Furthermore, only the lead researcher in this study will have access to this sensitive information.*

Your data will be kept for 10 years (standard retention time) after the research is concluded.

Your data *will* be stripped of your name and other information that can identify you, with the aim of keeping your brain activity confidential as is your right.

If you agree that Leiden University can further use of your personal data for other research in the field of Brain-Computer Interfaces, within 6 months after the end of this research, your data will be used for this research as well. Please indicate this below.

Your rights

Within the European privacy law, you have several rights. For instance: if you change your mind about your participation, you can send an e-mail with a short message indicating that you want your personal data to be removed, then your name will be permanently deleted from the collected data.

Other rights are, for instance, the right to be informed and the right to rectify. If you want to know more about your rights: these are listed in chapter 3 of the GDPR, in which articles 15 to 21 are the most relevant ones in this case.

- If you have any questions or concerns, please contact:

  Mohamad Hoteit, Leiden Institute of Advanced Computer Science, Leiden University.

  m.hoteit@umail.leidenuniv.nl Tel: +31 6 47 25 08 72

- If you or you guardian have any questions that you would like to address to an independent qualified party, please contact:

  Richard van Dijk, Leiden Institute of Advanced Computer Science, Leiden University.
  m.k.van.dijk@liacs.leidenuniv.nl

  Matthijs van Leeuwen, Leiden Institute of Advanced Computer Science, Leiden University.
  m.van.leeuwen@liacs.leidenuniv.nl

  Tessa Verhoef, Leiden Institute of Advanced Computer Science, Leiden University.
  t.verhoef@liacs.leidenuniv.nl

In case your data is used for further research you will receive a notification of this, with the possibility to withdraw your consent. Please place a cross in the box that is applicable.

O I do not consent to any use of the information collected about me.

O I consent to the use of the information collected about me for this research project, but not for further research.

O I consent to the use of the information collected about me for this research project, as well as for further research in the field of Human interaction research, brain interface research.

Name ____________________

Date ____________________

Location ____________________

Signature ____________________

Appendix B

Personal Information

Research Study Participant Information Form

Title of the Study: Decoding 3D Upper Limb Motion Using EEG and Motion Capture Integration: A Deep Learning Approach.

Principal Investigator: Mohamad Hoteit, Leiden Institute of Advanced Computer Science, Leiden University

Purpose of This Form: This form is designed to collect necessary personal data from participants involved in the research study. The information you provide here will be kept confidential and used solely for the purposes described in the consent form.

Personal Information

First Name: ___________________________________

Last Name: ___________________________________

E-mail Address: ___________________________________

Gender: ___________________________________

Age: ___________________________________

Note:

- Please specify your biological birth gender. This is important because Male and Female brains are quite different under EEG studies.

Appendix C

Participant Instructions

Checklist for instructions to participants

1. Give information regarding the aim of the study:

- The goal of the research is to identify brain activity which maps to the movement of your upper limbs.

2. Information regarding the registration:

- We register EEG from the brain. It is very important that you sit as still as possibly.

- Avoid additional muscle activity. Don't talk during the performance of the task.

- Focus on the task.

- We will register where the hand, elbow, and shoulder (right) are during the execution of the task.

- There are no known risks with the experiments.

3. Describe the task

- Sit close to the table, relax your shoulder, and place your arms next to your body on the chair's armrests. During the execution of the task, the forearm shall not touch the table. The other arm should rest on the armrest.

- The audio tone is the signal to reach out towards the target. A different audio tone will be used as signal to bring back your arm to the rest position.

- You shall rest your hand on the armrest – relax your shoulder.

- Before we start the registration you will get to practice the task a few times.

4. Risk and voluntary participation

- The participation is voluntary, and you may quit at any time.

- If you have any questions, feel free to ask before we start (or between the tasks).

5. Consent form

Ensure that the participant signs the consent form.

Appendix D

Kinesthetic and Visual Imagery Questionnaire

Kinesthetic and Visual Imagery Questionnaire - Short Version (KVIQ-10)

Overview

The KVIQ-10 is a tool used to assess an individual's ability to imagine movements visually (clarity of the image) and kinesthetically (intensity of sensations). It is designed for use in seated participants, making it suitable for both clinical and non-clinical populations. The questionnaire evaluates five movements for both visual and kinesthetic imagery, providing scores on two subscales.

Instructions

This questionnaire asks you to imagine performing specific movements in two ways:

1. **Visual Imagery**: Attempt to form a visual image of the movement in your mind. Imagine yourself performing the movement as if you are watching yourself.
2. **Kinesthetic Imagery**: Attempt to feel what performing the movement is like without actually doing it. Imagine the sensation of the movement as vividly as possible.

For each movement:

1. You will first perform the movement as demonstrated by the examiner.
2. You will return to the starting position and imagine performing the movement:
    - First, rate how clearly you can **see** the movement (visual imagery).
    - Next, rate how intensely you can **feel** the movement (kinesthetic imagery).
3. Use the provided rating scales to assess each dimension of imagery.

Rating Scales

Visual Imagery Scale		**Kinesthetic Imagery Scale**	
Rating Description			
5	Image as clear as seeing	**5**	Sensation as intense as executing
4	Clear image	**4**	Intense sensation
3	Moderately clear image	**3**	Moderately intense sensation
2	Blurred image	**2**	Mildly intense sensation
1	No image	**1**	No sensation

Movements

1. Forward Shoulder Flexion

- **Starting Position**: Sit upright with your arm resting at your side.
- **Action**: Move your arm forward and upward until it is at shoulder height, then return to the starting position.
- **Imagery Task**:
  - Visual: Imagine seeing your arm move forward and upward.
  - Kinesthetic: Imagine feeling the motion of your arm as it moves forward.

2. Thumb-Finger Opposition

- **Starting Position**: Sit upright with your hand resting on your lap.
- **Action**: Sequentially touch the tip of your thumb to the tip of each finger on the same hand, then return to the starting position.
- **Imagery Task**:
  - Visual: Imagine seeing your thumb touch each fingertip.
  - Kinesthetic: Imagine feeling the contact of your thumb with each finger.

3. Forward Trunk Flexion

- **Starting Position**: Sit upright with your feet flat on the floor.
- **Action**: Slowly bend forward at the hips as if reaching for your toes, then return to the starting position.
- **Imagery Task**:
  - Visual: Imagine seeing yourself bend forward.
  - Kinesthetic: Imagine feeling the stretch and movement as you bend.

4. Hip Abduction

- **Starting Position**: Sit upright with your knees bent and feet flat on the floor.
- **Action**: Move one leg outward to the side, keeping your foot on the floor, then return to the starting position.
- **Imagery Task**:
  - Visual: Imagine seeing your leg move outward.
  - Kinesthetic: Imagine feeling the sensation of your leg moving.

5. Foot Tapping

- **Starting Position**: Sit upright with your feet flat on the floor.
- **Action**: Lift your foot slightly and tap it on the floor repeatedly, then return to the starting position.
- **Imagery Task**:
    - Visual: Imagine seeing your foot lift and tap.
    - Kinesthetic: Imagine feeling the motion of your foot tapping.

Response Form

Movement	Visual Rating (1–5)	Kinesthetic Rating (1–5)
1. Forward Shoulder Flexion		
2. Thumb-Finger Opposition		
3. Forward Trunk Flexion		
4. Hip Abduction		
5. Hip Abduction		

Scoring Instructions

1. **Subscale Scores**:
    - Visual Imagery Subscale (V): Sum of visual ratings for all five movements (maximum = 25).
    - Kinesthetic Imagery Subscale (K): Sum of kinesthetic ratings for all five movements (maximum = 25).
2. **Total Score**:
    - Add the visual and kinesthetic subscale scores (maximum = 50).

Appendix E

Ethical Approval

Universiteit Leiden

Faculty of Science
Ethics Review Committee

Gorlaeus laboratory
Einsteinweg 55
2333 CC Leiden

Richard M.K. van Dijk

Number	2024 - 012	*Date*	11 July 2024
Your reference		*Telephone*	
Subject	Ethics Review Committee	*Contact*	M. Leemkuil

Project title	Decoding 3D Kinematics from EEG with a Biomechanical model and Interactive Machine Learning.
Applicants	Richard M.K. van Dijk, M. Hoteit (student)

Dear colleague,

The committee has considered your proposal 'Decoding 3D Kinematics from EEG with a Biomechanical model and Interactive Machine Learning.'and concludes that the research proposed adheres to the ethics principles of Leiden University.

The proposal concerns an experimental collection of ECG data and motion data from adult participants. This is a preliminary study that potentially will not yield conclusive results (due to a small sample size) but is a precursor for future larger studies. The study does not entail a big risk or burden on the participants, and so we think it can be approved.
However, you might consider whether the sample is sufficient to obtain conclusive results, given the potential gender, cultural background and mobility diversity among the participants, and perhaps perform a study with a slightly larger group of people (e.g. 10 instead of 5). We consider that a small increase in the sample will still fall under this application.

Yours sincerely
On behalf of the Ethics Review Committee

Prof.dr. S. Verberne
Chair

Appendix F

Invitation Flyer

Think It, Move It: Unlock the Future of Interaction!

Call For Participants!

Study Description
Participants will perform a series of tasks involving real and imagined arm movements while wearing an EEG cap and a Motion Capture suit to record brain activity and motion parameters simultaneously. You will be guided through the tasks, and your data will help us develop a brain-computer interfaces.

Eligibility
•Age: 18-35
•Right-handed
•Healthy: No medication
•Compensation provided

Location & Duration
•Sylvius, Lab 2.4.01
•About 90 mins

Sign Up Now!

https://forms.gle/qcH9GP1fbwh2B2J29

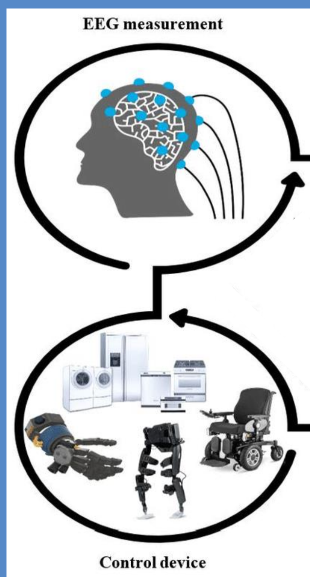

Bibliography

Víctor Asanza, Enrique Peláez, Francis Loayza, Leandro L. Lorente-Leyva, and Diego H. Peluffo-Ordóñez. Identification of lower-limb motor tasks via brain–computer interfaces: A topical overview. *Sensors*, 22(5), 2022. ISSN 1424-8220. doi: 10.3390/s22052028. URL https://www.mdpi.com/1424-8220/22/5/2028.

Shikhar Bahl, Mustafa Mukadam, Abhinav Gupta, and Deepak Pathak. Neural dynamic policies for end-to-end sensorimotor learning, 2020. URL https://arxiv.org/abs/2012.02788.

Ou Bai, Peter Lin, Sherry Vorbach, Mary Kay Floeter, Noriaki Hattori, and Mark Hallett. A high performance sensorimotor beta rhythm-based brain–computer interface associated with human natural motor behavior. *Journal of Neural Engineering*, 5(1):24, dec 2007. doi: 10.1088/1741-2560/5/1/003. URL https://dx.doi.org/10.1088/1741-2560/5/1/003.

Biosemi B.V. Biosemi trigger interface. URL https://www.biosemi.com/faq/USB%20Trigger%20interface%20cable.htm. Accessed: Accessed: 2024-12-14.

BioSemi B.V. Headcap electrode placement, n.d. URL https://www.biosemi.com/headcap.htm. Accessed: 2024-12-27.

Christian Cajochen, Daniel P Brunner, Kurt Krauchi, Peter Graw, and Anna Wirz-Justice. Eeg and subjective sleepiness during extended wakefulness in different circadian phases. *Electroencephalography and Clinical Neurophysiology*, 94(5):349–355, 1995.

SueYeon Chung and L.F. Abbott. Neural population geometry: An approach for understanding biological and artificial neural networks. *Current Opinion in Neurobiology*, 70:137–144, October 2021. ISSN 0959-4388. doi: 10.1016/j.conb.2021.10.010. URL http://dx.doi.org/10.1016/j.conb.2021.10.010.

Cameron Condylis, Eric Lowet, Jianguang Ni, Karina Bistrong, Timothy Ouellette, Nathaniel Josephs, and Jerry L. Chen. Context-dependent sensory processing across primary and secondary somatosensory cortex. *Neuron*, 106(3):515–525.e5, 2020. ISSN 0896-6273. doi: https://doi.org/10.1016/j.neuron.2020.02.004. URL https://www.sciencedirect.com/science/article/pii/S0896627320301033.

Hengchang Dai, Xi Liu, Jingbin Lu, Yuncheng Lu, Yueming Zhang, and Jianqiang Zhang. A survey of eeg and machine learning-based methods for neural rehabilitation. *IEEE Transactions on Neural Systems and Rehabilitation Engineering*, 31:2828–2846, 2023. doi: 10.1109/TNSRE.2023.3302132.

Antonio Delgado-Aguilera, Pedro Moreno-Briseño, et al. Age-related differences in reaching behavior: A spatiotemporal analysis of upper-limb kinematics. *Journal of Motor Behavior*, 2024. In press.

Guillaume Durandau, Dario Farina, and Massimo Sartori. Robust real-time musculoskeletal modeling driven by electromyograms. *IEEE Transactions on Biomedical Engineering*, 65 (3):556–564, 2018. doi: 10.1109/TBME.2017.2704085.

Robert E Dustman, David E Shearer, and R Yale Emmerson. Age-related changes in eeg slowing during performance of cognitive tasks. *Neurobiology of Aging*, 20(5):421–432, 1999.

B. J. Edelman, J. Meng, D. Suma, C. Zurn, E. Nagarajan, B. S. Baxter, C. C. Cline, and B. He. Noninvasive neuroimaging enhances continuous neural tracking for robotic device control. *Science Robotics*, 4(31):eaaw6844, 2019. doi: 10.1126/scirobotics.aaw6844. URL https://www.science.org/doi/abs/10.1126/scirobotics.aaw6844.

Edward V. Evarts. Motor cortex reflexes associated with learned movement. *Science*, 179 (4072):501–503, 1973.

Karl Friston. The free-energy principle: a unified brain theory? *Nature Reviews Neuroscience*, 11(2):127–138, 2010.

Mononito Goswami, Konrad Szafer, Arjun Choudhry, Yifu Cai, Shuo Li, and Artur Dubrawski. Moment: A family of open time-series foundation models, 2024. URL https://arxiv.org/abs/2402.03885.

Adam Gosztolai, Robert L. Peach, Alexis Arnaudon, Mauricio Barahona, and Pierre Vandergheynst. Marble: Interpretable representations of neural population dynamics using geometric deep learning. *Nature Methods*, 22(3):612–620, 2025. ISSN 1548-7105. doi: 10.1038/s41592-024-02582-2. URL https://doi.org/10.1038/s41592-024-02582-2.

Takashi Hanakawa, Ilka Immisch, Keiichiro Toma, Michael A. Dimyan, Peter Van Gelderen, and Mark Hallett. Functional properties of brain areas associated with motor execution and imagery. *Journal of Neurophysiology*, 89(2):989–1002, 2003. doi: 10.1152/jn.00132.2002. URL https://doi.org/10.1152/jn.00132.2002. PMID: 12574475.

Nora A. Herweg and Michael J. Kahana. Spatial representations in the human brain. *Frontiers in Human Neuroscience*, 12, 2018. ISSN 1662-5161. doi: 10.3389/fnhum.2018.00297. URL https://www.frontiersin.org/journals/human-neuroscience/articles/10.3389/fnhum.2018.00297.

Guy Hotson, Ryan J. Smith, Adam G. Rouse, Marc H. Schieber, Nitish V. Thakor, and Brock A. Wester. High precision neural decoding of complex movement trajectories using recursive bayesian estimation with dynamic movement primitives. *IEEE Robotics and Automation Letters*, 1(2):676–683, 2016. doi: 10.1109/LRA.2016.2516590.

Movella Inc. Mt manager, 2014. URL https://mtidocs.movella.com/mt-manager. Accessed: 2024-12-8.

Ji-Hoon Jeong, Kyung-Hwan Shim, Dong-Joo Kim, and Seong-Whan Lee. Brain-controlled robotic arm system based on multi-directional cnn-bilstm network using eeg signals. *IEEE Transactions on Neural Systems and Rehabilitation Engineering*, 28(5):1226–1238, 2020. doi: 10.1109/TNSRE.2020.2981659.

Wei-Bang Jiang, Li-Ming Zhao, and Bao-Liang Lu. Large brain model for learning generic representations with tremendous eeg data in bci, 2024. URL https://arxiv.org/abs/2405.18765.

Mads Jochumsen, Imran Khan Niazi, Denise Taylor, Dario Farina, and Kim Dremstrup. Detecting and classifying movement-related cortical potentials associated with hand movements in healthy subjects and stroke patients from single-electrode, single-trial eeg. *Journal of Neural Engineering*, 12(5):056013, aug 2015. doi: 10.1088/1741-2560/12/5/056013. URL https://dx.doi.org/10.1088/1741-2560/12/5/056013.

Justin Kilmarx, Ivan Tashev, José del R. Millán, James Sulzer, and Jarrod Lewis-Peacock. Evaluating the feasibility of visual imagery for an eeg-based brain–computer interface. *IEEE Transactions on Neural Systems and Rehabilitation Engineering*, 32:2209–2219, 2024. doi: 10.1109/TNSRE.2024.3410870.

Jeong-Hun Kim, Felix Bießmann, and Seong-Whan Lee. Decoding three-dimensional trajectory of executed and imagined arm movements from electroencephalogram signals. *IEEE Transactions on Neural Systems and Rehabilitation Engineering*, 23(5):867–876, 2015. doi: 10.1109/TNSRE.2014.2375879.

Reinmar J Kobler, Andreea I Sburlea, Valeria Mondini, Masayuki Hirata, and Gernot R Müller-Putz. Distance- and speed-informed kinematics decoding improves m/eeg based upper-limb movement decoder accuracy. *Journal of Neural Engineering*, 17(5):056027, oct 2020. doi: 10.1088/1741-2552/abb3b3. URL https://dx.doi.org/10.1088/1741-2552/abb3b3.

Attila Korik, Ronen Sosnik, Nazmul Siddique, and Damien Coyle. Decoding imagined 3d arm movement trajectories from eeg to control two virtual arms—a pilot study. *Frontiers in Neurorobotics*, 13, 2019. ISSN 1662-5218. doi: 10.3389/fnbot.2019.00094. URL https://www.frontiersin.org/journals/neurorobotics/articles/10.3389/fnbot.2019.00094.

Christian A. Kothe. Lab streaming layer (lsl), 2014. URL https://github.com/sccn/labstreaminglayer. Accessed: 2024-11-29.

Li-Wei Liao, Chia-Tai Wang, Yu-Han Chen, Jyun-Ying Chang, and Chin-Teng Lin. Novel dry electrode for eeg recording with good signal quality and usability. *Sensors*, 11(6):5396–5410, 2011.

Dong Liu, Weihai Chen, Kyuhwa Lee, Ricardo Chavarriaga, Fumiaki Iwane, Mohamed Bouri, Zhongcai Pei, and José del R. Millán. Eeg-based lower-limb movement onset decoding: Continuous classification and asynchronous detection. *IEEE Transactions on Neural Systems and Rehabilitation Engineering*, 26(8):1626–1635, 2018. doi: 10.1109/TNSRE.2018.2855053.

F Lotte, L Bougrain, A Cichocki, M Clerc, M Congedo, A Rakotomamonjy, and F Yger. A review of classification algorithms for eeg-based brain–computer interfaces: a 10 year update. *Journal of Neural Engineering*, 15(3):031005, apr 2018. doi: 10.1088/1741-2552/aab2f2. URL https://dx.doi.org/10.1088/1741-2552/aab2f2.

Matthew D. Luciw, Ewa Jarocka, and Benoni B. Edin. Multi-channel eeg recordings during 3,936 grasp and lift trials with varying weight and friction. *Scientific Data*, 1(1):140047, 2014. ISSN 2052-4463. doi: 10.1038/sdata.2014.47. URL https://doi.org/10.1038/sdata.2014.47.

Francine Malouin, Carol L Richards, Philip L Jackson, Francine Dumas, and Julien Doyon. Kinesthetic and visual imagery questionnaire (kviq) for assessing motor imagery in persons with physical disabilities: a reliability and construct validity study. *Journal of Neurologic Physical Therapy*, 34(2):65–75, 2010.

Alexander Mathis, Pranav Mamidanna, Kevin M Cury, Tiberiu Abe, Venkatesh N Murthy, Mackenzie W Mathis, and Matthias Bethge. Deeplabcut: markerless pose estimation of user-defined body parts with deep learning. *Nature Neuroscience*, 21(9):1281–1289, 2018. doi: 10.1038/s41593-018-0209-y.

Christoph M. Michel and Thomas Koenig. Eeg microstates as a tool for studying the temporal dynamics of whole-brain neuronal networks: A review. *NeuroImage*, 180:577–593, 2018. ISSN 1053-8119. doi: https://doi.org/10.1016/j.neuroimage.2017.11.062. URL https://www.sciencedirect.com/science/article/pii/S105381191731008X. Brain Connectivity Dynamics.

Movella Inc. Xsens mvn awinda motion capture system, 2023a. URL https://www.movella.com/products/motion-capture/xsens-mvn-awinda. Accessed: 2025-04-01.

Movella Inc. Synchronising xsens with ant neuro eeg systems, 2023b. URL https://www.movella.com/hubfs/Downloads/plugins%20%20tools/SynchronisingXsenswithANTneuro.pdf. Accessed: 2025-05-13.

Movella Inc. *MVN User Manual*, 2023c. URL https://www.movella.com/hubfs/MVN_User_Manual.pdf. Accessed: 2025-05-13.

Christa Neuper, Reinhold Scherer, Miriam Reiner, and Gert Pfurtscheller. Imagery of motor actions: Differential effects of kinesthetic and visual–motor mode of imagery in single-trial eeg. *Cognitive Brain Research*, 25(3):668–677, 2005. ISSN 0926-6410. doi: https://doi.org/10.1016/j.cogbrainres.2005.08.014. URL https://www.sciencedirect.com/science/article/pii/S0926641005002533.

R C Oldfield. The assessment and analysis of handedness: The edinburgh inventory. *Neuropsychologia*, 9(1):97–113, 1971.

Maarten C. Ottenhoff, Maxime Verwoert, Sophocles Goulis, Simon Tousseyn, Johannes P. van Dijk, Maryam M. Shanechi, Omid G. Sani, Pieter Kubben, and Christian Herff. Decoding continuous goal-directed movement from human brain-wide intracranial recordings. *bioRxiv*, 2025. doi: 10.1101/2025.02.05.636287. URL https://www.biorxiv.org/content/early/2025/02/06/2025.02.05.636287.

David Pagnon, Steffen Willwacher, Mathieu Sanno, and Harald Bohm. Pose2sim: An end-to-end workflow for 3d markerless sports kinematics—part 1: Robustness. *Frontiers in Sports and Active Living*, 4:849099, 2022. doi: 10.3389/fspor.2022.849099.

Joseph Paillard, Jörg F. Hipp, and Denis A. Engemann. Green: a lightweight architecture using learnable wavelets and riemannian geometry for biomarker exploration. *bioRxiv*, 2024. doi: 10.1101/2024.05.14.594142. URL https://www.biorxiv.org/content/early/2024/05/14/2024.05.14.594142.

Sidharth Pancholi, Amita Giri, Anant Jain, Lalan Kumar, and Sitikantha Roy. Source aware deep learning framework for hand kinematic reconstruction using eeg signal. *IEEE Transactions on Cybernetics*, 53(7):4094–4106, 2022. doi: 10.1109/TCYB.2022.3166604.

Chethan Pandarinath, Daniel J O'Shea, Jennifer Collins, and et al. Inferring single-trial neural population dynamics using sequential autoencoders. *Nature Methods*, 15(10):805–815, 2018.

G. Pfurtscheller, C. Brunner, A. Schlögl, and F.H. Lopes da Silva. Mu rhythm (de)synchronization and eeg single-trial classification of different motor imagery tasks. *NeuroImage*, 31(1):153–159, 2006. ISSN 1053-8119. doi: https://doi.org/10.1016/j.neuroimage.2005.12.003. URL https://www.sciencedirect.com/science/article/pii/S1053811905025140.

Neethu Robinson, Cuntai Guan, and A P Vinod. Adaptive estimation of hand movement trajectory in an eeg based brain–computer interface system. *Journal of Neural Engineering*, 12(6): 066019, oct 2015. doi: 10.1088/1741-2560/12/6/066019. URL https://dx.doi.org/10.1088/1741-2560/12/6/066019.

Neethu Robinson, Tan Wei Jie Chester, and Smitha KG. Use of mobile eeg in decoding hand movement speed and position. *IEEE Transactions on Human-Machine Systems*, 51(2):120–129, 2021. doi: 10.1109/THMS.2021.3056274.

Kaushik Roy, Oguz Sani, and Pouya Bashivan. Chrononet: A deep recurrent neural network for decoding eeg signals. *IEEE Transactions on Neural Networks and Learning Systems*, 2022. doi: 10.1109/TNNLS.2022.3225478.

Matteo Saveriano, Fares J Abu-Dakka, Aljaž Kramberger, and Luka Peternel. Dynamic movement primitives in robotics: A tutorial survey. *The International Journal of Robotics Research*, 42(13):1133–1184, September 2023. ISSN 1741-3176. doi: 10.1177/02783649231201196. URL http://dx.doi.org/10.1177/02783649231201196.

SOLO Labs. Usbparmarker – markers and events. URL https://researchwiki.solo.universiteitleiden.nl/xwiki/wiki/researchwiki.solo.universiteitleiden.nl/view/Hardware/Markers%20and%20Events/UsbParMarker/. Accessed: Accessed: 2024-12-14.

Ronen Sosnik and Li Zheng. Reconstruction of hand, elbow and shoulder actual and imagined trajectories in 3d space using eeg current source dipoles. *Journal of Neural Engineering*, 18 (5):056011, apr 2021. doi: 10.1088/1741-2552/abf0d7. URL https://dx.doi.org/10.1088/1741-2552/abf0d7.

Alessandro Marin Vargas, Axel Bisi, Alberto Chiappa, Chris Versteeg, Lee Miller, and Alexander Mathis. Task-driven neural network models predict neural dynamics of proprioception. *bioRxiv*, 2023. doi: 10.1101/2023.06.15.545147. URL https://www.biorxiv.org/content/early/2023/06/16/2023.06.15.545147.

Christopher Wang, Vighnesh Subramaniam, Adam Uri Yaari, Gabriel Kreiman, Boris Katz, Ignacio Cases, and Andrei Barbu. Brainbert: Self-supervised representation learning for intracranial recordings, 2023a. URL https://arxiv.org/abs/2302.14367.

Jiarong Wang, Luzheng Bi, Weijie Fei, and Kun Tian. Eeg-based continuous hand movement decoding using improved center-out paradigm. *IEEE Transactions on Neural Systems and Rehabilitation Engineering*, 30:2845–2855, 2022. doi: 10.1109/TNSRE.2022.3211276.

Jiarong Wang, Luzheng Bi, and Weijie Fei. Eeg-based motor bcis for upper limb movement: Current techniques and future insights. *IEEE Transactions on Neural Systems and Rehabilitation Engineering*, 31:4413–4427, 2023b. doi: 10.1109/TNSRE.2023.3330500.

P Wang et al. Mtrt: Motion trajectory reconstruction transformer for eeg-based bci decoding. *IEEE Transactions on Neural Systems and Rehabilitation Engineering*, 31:2349–2358, May 2023c.

Mengqi Xing, Olusola Ajilore, Ouri E. Wolfson, Christopher Abbott, Annmarie MacNamara, Reza Tadayonnejad, Angus Forbes, K. Luan Phan, Heide Klumpp, and Alex Leow. Thought chart: Tracking dynamic eeg brain connectivity with unsupervised manifold learning. In Giorgio A. Ascoli, Michael Hawrylycz, Hesham Ali, Deepak Khazanchi, and Yong Shi, editors, *Brain Informatics and Health*, pages 149–157, Cham, 2016. Springer International Publishing. ISBN 978-3-319-47103-7.

Nobuaki Yoshimura, Hiroki Tsuda, Tomoyuki Kawase, Hiroki Mito, Yasuharu Hasegawa, Masaki Takahashi, and Yasuharu Koike. Decoding finger movement in humans using synergy of eeg cortical current signals. *Scientific Reports*, 7:11382, 2017. doi: 10.1038/s41598-017-09770-5. URL https://doi.org/10.1038/s41598-017-09770-5.

ZeroKey Inc. Quantum rtls, 2023. URL https://zerokey.com/quantum-rtls/. Accessed: 2025-04-01.

Daoze Zhang, Zhizhang Yuan, Yang Yang, Junru Chen, Jingjing Wang, and Yafeng Li. Brant: Foundation model for intracranial neural signal. In *Thirty-seventh Conference on Neural Information Processing Systems*, 2023. URL https://openreview.net/forum?id=DDkl9vaJyE.